https://doi.org/10.5194/egusphere-2023-1403
Preprint. Discussion started: 28 June 2023
© Author(s) 2023. CC BY 4.0 License.

Drivers of Laptev Sea interannual variability in salinity and temperature

Phoebe A. Hudson[1, 2], Adrien C. H. Martin[2, 3], Simon A. Josey[2], Alice Marzocchi[2], Athanasios Angeloudis[1]

[1] University of Edinburgh, Edinburgh UK

[2] National Oceanography Center, Southampton, UK

[3] NOVELTIS, Labège, France

Correspondence to: Phoebe A Hudson (PA.Hudson@sms.ed.ac.uk)

Abstract. Eurasian Rivers provide a quarter of total fresh water to the Arctic, maintaining a persistent fresh layer that covers the surface Arctic Ocean. The Lena River supplies the largest volume of runoff and plays a key role in this system, as runoff outflows into the Laptev Sea as a particularly shallow plume. This freshwater export controls Arctic Ocean stratification, circulation, and basin-wide sea ice area. Previous in-situ and modelling studies suggest that local wind forcing is a primary driver of variability in Laptev sea surface salinity (SSS) with no consensus over the roles of Lena river discharge and sea ice cover in contributing to this variability. Until recently, satellite SSS retrievals were insufficiently accurate for use in the Arctic, due to the low sensitivity of the L-band signal they utilise in cold water and challenges of retrieval near sea ice. However, retreating sea ice cover and continuous progress in satellite product development have significantly improved SSS retrievals, giving satellite SSS data true potential in the Arctic.

This study demonstrates a novel method of using satellite-based SSS, sea surface temperature (SST) data, in-situ observations, and reanalysis products to identify the dominant drivers of interannual variability in Laptev Sea dynamics. Satellite-based SSS is found to agree well with in-situ data in this region ($r > 0.8$) and provides notable improvements compared to the reanalysis product used in this study ($r > 0.7$) in capturing patterns and variability observed in in-situ data. The satellite SSS data firmly establishes what has previously been subject to debate due to the limited years and locations analysed with in-situ data: that the zonal wind is the dominant driver of offshore or onshore Lena river plume transport. This finding is affirmed by the strong agreement in SSS pattern in all reanalyses and satellite products used in this study under eastward and westward wind regimes. The pattern of SST also varies with the zonal wind component, and drives spatial variability in sea ice area. The strong correspondence between large scale and local zonal wind dynamics and the key role of SSS and SST variability in driving sea ice and stratification dynamics demonstrates the importance of changes in large-scale atmospheric dynamics for variability in this region as well as for future Arctic sea ice dynamics and freshwater transport.

https://doi.org/10.5194/egusphere-2023-1403
Preprint. Discussion started: 28 June 2023
© Author(s) 2023. CC BY 4.0 License.

Key Points:

- Better agreement between in-situ measurements and satellite based sea surface salinity (SSS) measurements compared to the 1/12° GLORYS12V1 reanalysis SSS or other reanalysis considered.
- The zonal wind component is the dominant driver of Lena river plume transport, with strong agreement across all products.
- The eastward wind confines the plume to the southern Laptev Sea and drives alongshore transport into the East Siberian Sea and westward wind drives offshore plume transport towards the northern Laptev Sea.
- Patterns of SST, sea ice concentration and area all co-vary with the zonal wind component.

1 Introduction:

Arctic river runoff represents over 10% of the total global river runoff, creating a fresh layer that covers the Arctic Ocean. This runoff is a key contribution to the Arctic halocline, the cold, fresh layer that sits above inflowing warm and salty Atlantic and Pacific Water. This fresh surface layer governs Arctic Ocean circulation and sea ice cover by preventing heat exchange between the underlying Atlantic Water and the overlying sea ice, limiting melt and strengthening the existing sea ice barrier to atmosphere-ocean momentum transfer. Of this runoff, Eurasian rivers contribute a quarter of the total fresh water to the Arctic Ocean, predominantly to the Kara and Laptev Seas. River runoff is suggested to be the driving cause of decadal variability in salinity over the Eurasian shelf seas (Steele and Ermold, 2004) and has the potential to alter considerably with climate change.

However, untangling the impact of the many changes that have already been observed with climate change poses a challenge. The dramatically warming Arctic surface air temperatures have already altered Arctic atmospheric circulation and brought ocean warming, an intensification of the hydrological cycle, snow and ice melt, and increases in river runoff (Overland and Wang, 2010; Prowse et al., 2015). These changes have the potential to drive enhanced stratification with increases in freshwater input (in the form of runoff and precipitation), or increased mixing (with the loss of sea ice and resulting increasing atmosphere-ocean heat and momentum transfer) (IPCC (Intergovernmental Panel on Climate Change), 2019). Understanding the interplay between these changes is crucial for predicting the future state of the Arctic system.

1.1 Laptev Sea

The Laptev Sea, within the Eurasian Arctic (Figure 1), provides an ideal region to study the interactions between these changes, given it's a hotspot of Arctic warming, sea ice loss, and increases in river runoff (Kraineva and Golubeva, 2022; Stadnyk et al., 2021). Changes in this region will likely have considerable influence on the wider Arctic as the Laptev Sea is a key region of Arctic sea ice production and dominant contributor to Arctic-wide thermohaline structure, including to the surface Transpolar Drift and to the Beaufort Gyre (Johnson and Polyakov, 2001; Morison et al., 2012; Reimnitz et al., 1994; Thibodeau et al., 2014). The combination of these changes will also have considerable local impacts, including by increasing coastal erosion, altering nutrient availability and primary productivity (Juhls et al., 2020; Nielsen et al., 2020; Paffrath et al., 2021; Polyakova et al., 2021).

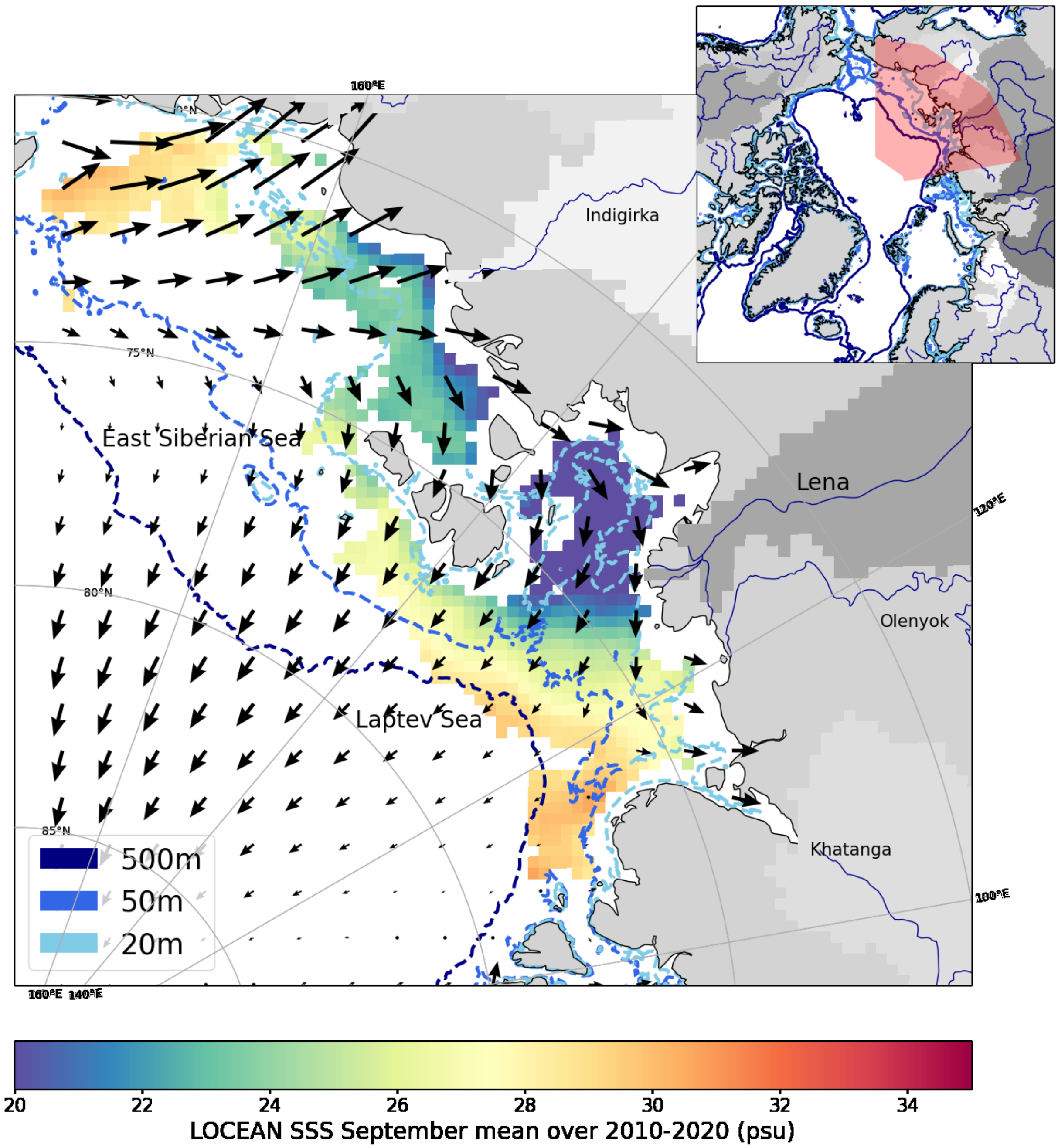

70 **Figure 1 : 2010-2020 LOCEAN SMOS satellite mean September SSS with GEBCO bathymetry contours for 20m, 50m and 500m overlaid in blue with mean 2010-2020 ERA5 June-September wind overlaid over the ocean. The inset in the top right corner depicts Arctic wide GEBCO bathymetry and the location of this region within the wider Arctic in red.**

https://doi.org/10.5194/egusphere-2023-1403
Preprint. Discussion started: 28 June 2023
© Author(s) 2023. CC BY 4.0 License.

The Laptev Sea primarily receives runoff from the Lena River, the largest river in the Arctic, which outflows as a particularly shallow plume due to the very shallow (2-3m) nature of the Lena Delta (Are and Reimnitz, 2000). Lena River fresh water dominates the spatial pattern of Laptev sea surface salinity (SSS) and is the main control on stratification in this region (Janout et al., 2020). Lena runoff is very seasonal, with very low flow throughout the winter, when the Lena River is partially frozen, and a strong peak between May and June following the melt of snow and land ice (Shiklomanov et al., 2021; Wang et al., 2021). Other rivers in this region, including the Khatanga, Olenyok and Indigirka, also contribute fresh water to the Laptev but all combined provide a five times smaller contribution than the Lena (Pasternak et al., 2022). Kara Sea fresh water can also contribute riverine fresh water to some of the western and northern Laptev shelf via the Vilkitsky Straight but contributions vary considerably interannually and are typically only a small component of the overall make-up (<25%) (Janout et al., 2020, 2015). Sea ice melt also provides fresh water to the Laptev Sea but has a negligible impact in summer/autumn as the freshwater contribution from sea ice melt is several orders of magnitudes smaller than the contribution from the Lena river (Dubinina et al., 2017).

Laptev Sea surface fresh water is typically characterized by eastward (cyclonic) circulation and weak tidal influence (Fofonova et al., 2014; Timokhov, 1994). This fresh surface layer exhibits considerable interannual variability, varying in meridional extent by over 500km, and has been widely studied using in-situ data and model output (Anderson et al., 2004; Dmitrenko et al., 2005, 2008; Fofonova et al., 2014; Janout et al., 2020; Osadchiev et al., 2021). The shallow Laptev shelf (depth ~20-25m) is mostly controlled by wind forcing and bottom friction, and the strong stratification on this shallow shelf prevents a full Ekman spiral from developing and aligns the surface current ~45 degrees to the right of the wind (Dmitrenko et al., 2005; Kubryakov et al., 2016; Osadchiev et al., 2021; Zhuk and Kubryakov, 2021). River discharge variability has also been suggested as a secondary driver of fluctuations in freshwater content and plume structure (Horner-Devine et al., 2015). However, wind forcing is more widely suggested to be the dominant driver of variability on the shelf (Dmitrenko et al., 2005; Osadchiev et al., 2021).

Whilst Lena river water typically remains in the Laptev Sea for 2-3 years, its longer-term fate exhibits considerable variability as it can be transported out of the Laptev Sea either northward into the Transpolar Drift or eastward towards the Beaufort Gyre (Bauch et al., 2013; Johnson and Polyakov, 2001; Paffrath et al., 2021). Large-scale atmospheric circulation (and the Arctic Oscillation Index (AOI)) and the initial transport of the fresh layer have been suggested as the main controls on its eventual transit (Johnson and Polyakov, 2001; Morison et al., 2012).

1.2 Satellite SSS in the Arctic

Satellite acquisitions of SSS have only been around since 2010, with the launch of the ESA Soil Moisture and Ocean Salinity (SMOS) satellite (Font et al., 2010; Kerr et al., 2010). The ability to measure salinity from space provided an unprecedented synoptic view of freshwater transport and ocean density, previously only hinted at by the relatively sparse in-situ platforms and datasets. Since then, SMOS, Aquarius (2011–2015, (Lagerloef et al., 2008)), and newly SMAP (2015-present, (Piepmeier et al., 2017)), have been widely used for salinity studies around most of the globe (Dossa et al., 2021; Fournier et al., 2017). They have proved invaluable for understanding the water cycle including air/sea fluxes, river runoff, horizontal advection and vertical exchanges (Zika et al., 2015; Vinogradova et al., 2019; Reul et al., 2020).

In the Arctic, in-situ measurements of salinity have long been particularly sparse and infrequent due to the persistent sea ice cover that restricts access throughout most of the year. Satellite SSS would prove invaluable as salinity is the dominant driver of density at high latitudes and plays a key role in controlling transport around the Arctic. However, sea ice and the low sensitivity of L-band signal in cold water has historically made satellite SSS retrievals at high latitudes a challenge. Recent progress in satellite product development has considerably lowered bias by over 0.15 pss compared to in-situ data in the Arctic, increasing confidence in acquisitions and making satellite SSS data a valuable resource for Arctic studies (Fournier et al., 2019; Supply et al., 2020). In addition, retreating Arctic sea ice cover and rapid atmospheric warming increases the spatial cover of satellite based SSS measurements. Whilst SSS retrievals at high latitudes still have larger uncertainties relative to the rest of the globe, previous works have shown that accuracy is sufficient to capture regions with sharp SSS gradients, such as river plumes (Kubryakov et al., 2016; Olmedo et al., 2018; Supply et al., 2020; Tang et al., 2018; Zhuk and Kubryakov, 2021). The Laptev Sea provides an ideal region for gaining new insights from satellite SSS retrievals, as the Lena River outflows as a large, very fresh, shallow plume, which creates strong SSS gradients that are clearly observable from satellite SSS data.

2 Data and Methods

2.1 Data Products

2.1.1 Satellite data

To validate and identify strengths and weaknesses of satellite-based SSS measurements over the Laptev Sea, this study uses two SMOS and two SMAP products which are described below:

The two SMAP products are global products and are not specific for the Arctic: JPL (Jet Propulsion Laboratory) v5 and RSS v4 (Remote Sensing Systems). Given the SMAP satellite's later launch, the SMAP products are compared over 2015-04 to 2022-01. The SMAP JPL product provides a large coverage including close to the sea ice edge. To be comparable with other

https://doi.org/10.5194/egusphere-2023-1403
Preprint. Discussion started: 28 June 2023
© Author(s) 2023. CC BY 4.0 License.

products, data are masked to only include SSS where the uncertainty provided in the product is lower than one pss. No masking is used for the three other products.

The two SMOS products are Arctic-ocean focused products: the L3 BEC (Barcelona Expert Centre) Arctic+ v3.1 and L3 LOCEAN (Laboratory of Ocean and Climatology) Arctic v1.1 products (Martínez et al., 2021; Supply et al., 2020). Monthly means are calculated from the 3-day BEC product to enable comparison with the other monthly satellite products. Their common period of data availability is 2011-01 to 2019-12. The two SMOS products are regridded onto a regular 0.25° grid (consistent with the SMAP grid) for easier comparison with in-situ data and such that a satellite median product could be calculated from the four satellite SSS products.

The satellite median is then calculated as the median of these four products (gridded or regridded at 0.25° resolution). The masked JPL product is used to calculate this median.

SST measurements are taken from the gap-filled L4 CCI (Climate Change Initiative) SST CDR (Climate Data Record) v2.1 (Merchant et al., 2019). A monthly product of this data regridded at 0.1 ° resolution is used over the SSS satellite period (2010 to 2021).

2.1.2 Reanalyses

The 1/12 degree CMEMS GLORYS12V1 reanalysis (hereafter referred to as GLORYS12V1) (Jean-Michel et al., 2021) is used as a comparison dataset alongside the SMOS/SMAP and CCI products over the common observational periods (since 2011/2015) in this region. This reanalysis is chosen for its good representation of Arctic sea ice concentration and its previous application to salinity variability in the Subpolar North Atlantic and Arctic (Biló et al., 2022; Hall et al., 2021; Jean-Michel et al., 2021; Liu et al., 2022). For consistency with the satellite SSS products, the GLORYS12V1 reanalysis is regridded onto a 0.25° grid for comparison with in-situ data (glorys_rg).

The E.U. Copernicus Marine Service Information Global Ensemble Physics reanalysis products are also validated against in-situ data for comparison with GLORYS12V1 (Masina et al., 2017). These includes four ¼ degree reanalyses including: GLORYS2V4 from Mercator Ocean, ORAS5 from ECMWF, GloSea5 from Met Office, and C-GLORS05 from CMCC.

https://doi.org/10.5194/egusphere-2023-1403
Preprint. Discussion started: 28 June 2023
© Author(s) 2023. CC BY 4.0 License.

2.1.3 In-situ data

CTD casts from oceanographic cruises in the Laptev Sea were obtained for comparison with the satellite products from a number of sources (Table 1). Only observations in the upper 10m are used for comparison with satellite data. The same analysis was conducted using only data in the upper 5m with no significant improvement. The analysis shown here is for the upper 10m to retain as much data as possible.

Table 1: Cruises, vessels and time-periods of salinity and temperature in-situ data used for analysis of vertical profiles and comparison with satellite data

Cruise Name	Vessel	Time Period	Reference
UDASH dataset (incl NABOS cruises 2013, 2015)	Numerous	1980-2015	(Behrendt et al., 2017)
SWERUS-C3 expedition	Oden	15th July – 25th September 2014	(Bjork, 2017)
NABOS cruises 2018	Akademik Tryoshnikov	3rd -17th October 2018	(Polyakov and Rember, 2019)
	Akademik Lavrentyev Akademik Mstislav Keldysh	20th September – 20th October 2016 23rd September – 13th October 2019	Supplementary materials (Osadchiev et al., 2021)

2.2 Methods

2.2.1 Data comparison / validation

All satellite and reanalysis products described above are compared with in-situ data over 2015-2020. The regridded SMOS data and GLORYS12V1 reanalysis (on a 0.25° grid) are used for comparison with in-situ data. Both correlation coefficients and root-mean square difference (RMSD) values are calculated for each individual product at all collocations between in-situ data and that product. Correlation coefficients and RMSD values are also calculated only where all products have a collocation with in-situ data. However, over 2015-2020, few in-situ observations are collected sufficiently near the surface (< 10 m) over regions where all satellite products obtain an SSS measurement (only 37 collocations). Therefore, RMSDs and correlation coefficients are also calculated for SMOS products and reanalyses over the longer SMOS time period (2011-2020) to obtain

https://doi.org/10.5194/egusphere-2023-1403
Preprint. Discussion started: 28 June 2023
© Author(s) 2023. CC BY 4.0 License.

more collocations (228). JPL SMAP and LOCEAN SMOS have particularly high correlation coefficients and low RMSD values and agree well so are used for further analysis.

2.2.2 Drivers of interannual variability

This study focuses on September as the month of maximum open water area and hence the largest area of satellite data for comparison with in-situ data. Two Septembers are shown for comparison of how well interannual variability is captured in each satellite product: 2016, a year of predominant eastward wind and 2019, a year of predominant westward wind. This study does not consider variability in SSS below 20 pss due to the sparsity of in-situ observations with SSS values below this threshold.

ECMWF's 5th generation reanalysis of global weather and climate (ERA5) monthly eastward and northward turbulent surface stress is used to identify years of anomalous east/west and north/south wind stress (Hersbach et al., 2020). The mean eastward and northward turbulent surface stress are calculated for June to September over the Laptev Sea shelf: 120-160E, 70-80N. A four month mean is chosen in order to reduce the high temporal variability in wind stress (± 0.05 N m^{-2}) and only keep the lower frequency signal the ocean reacts to.

The 3 years of maximum and minimum eastward turbulent surface stress are identified for each of the two satellite periods (SMOS: 2011-2020 and SMAP : 2015-2022), in order to be able to calculate "eastward" and "westward" SSS and SST composites. The three years of maximum eastward turbulent surface stress are identified to be 2012, 2016 and 2017 over the SMOS timeseries, and identified to be 2016, 2017 and 2021 over the SMAP timeseries (Figure 4). Conversely, the three years of westward (minimum eastward) turbulent surface stress are identified to be 2011, 2013 and 2019 over the SMOS timeseries, and 2015, 2019 and 2020 over the SMAP timeseries.

The "eastward" SSS composite is then calculated as the mean of the three most eastward years for GLORYS12V1 SSS and LOCEAN SMOS (2012, 2016, 2017), and for JPL SMAP (2016, 2017, 2021). The "westward" SSS composite is calculated as the mean of the three most westward years for GLORYS12V1 SSS and LOCEAN SMOS (2011, 2013, 2019) and for JPL SMAP (2015, 2019, 2020). The same years are used to calculate "eastward" and "westward" SST composites using GLORYS12V1 SST and L4 v2.1 CCI SST as well as for GLORYS12V1 sea ice concentration.

The GLORYS12V1 sea ice area (SIA) in September in the Laptev Sea (defined to be between 120-145 °E and 68-85 °N for the purpose of calculating SIA) is calculated from GLORYS12V1 sea ice concentration for all years used in the (eastward and westward) composite analysis. The mean "eastward" and "westward" SIA is then calculated as the mean of SIA in the three most eastward and westward years respectively.

https://doi.org/10.5194/egusphere-2023-1403
Preprint. Discussion started: 28 June 2023
© Author(s) 2023. CC BY 4.0 License.

3 Results:

3.1 Comparison of SSS products

Table 2 : Correlation coefficients from in-situ SSS data < 10m over 2015-2020 (left) and 2011-2020 (right) with GLORYS12V1, BEC SMOS and LOCEAN SMOS products regridded at a 0.25 degree spatial resolution (glorys_rg, bec_rg, locean_rg), JPL SMAP in regions where the provided SSS uncertainty is less than 1 psu, RSS SMAP, the satellite SSS median product and the four CMEMS global ensemble reanalysis products: GLORYS2V4, ORAS5, GloSea5, and C-GLORS05. Correlation coefficients are calculated both at all points where an individual product is collocated with insitu data (All obsv <10m) and for only where all products had a collocation point near insitu data (Common obsv <10m). There are 37 collocations between all products over 2015-2020 and 228 collocations over 2011-2020.

	2015-2020				2011-2020			
	All obsv <10m		Common obsv <10m		All obsv <10m		Common obsv <10m	
	Num obsv	Corr coeff	Num obsv	Corr coeff	Num obsv	Corr coeff	Num obsv	Corr coeff
GLORYS12V1 regridded onto 0.25° grid	221	0.80		0.35	1692	0.78		0.62
BEC SMOS regridded onto 0.25° grid	90	0.52		0.64	277	0.63	228	0.67
LOCEAN SMOS regridded onto 0.25° grid	78	0.82		0.74	228	0.83		0.83
JPL SMAP (where uncertainty < 1 pss)	57	0.80		0.74				
RSS SMAP	41	0.65	37	0.58				
Satellite SSS median product	91	0.79		0.75				
C-GLORS05	219	0.76		0.03	1695	0.71		0.42
GloSea5	219	0.84		0.04	1695	0.87	228	0.65
GLORYS2V4	219	0.81		0.69	1695	0.70		0.40
ORAS5	219	0.85		0.44	1695	0.87		0.70

The satellites products show a good agreement with in-situ measurements within the top 10m, with a correlation coefficient typically higher than 0.62 and up to 0.83. The RMSD with in-situ is typically between 1.1 pss and 1.65 pss. Despite this relatively high error in RMSD, due to the large range of SSS observed over this small area (5 pss to 35 pss), both dataset are well correlated. JPL SMAP, LOCEAN SMOS, and the median sat product stand out as having particularly high correlation (r ~0.8) coefficients compared to all other products. Over the full SMOS period, the LOCEAN product correlates strongly with in-situ data (r = 0.83) but the BEC product is less strongly correlated (r = 0.67).

The collocated in-situ data (common obsv <10m) are all located in low sea ice regions (<30% sea ice concentration), where satellite SSS retrievals are possible. Over the Laptev Sea, the strong horizontal gradient in SSS maintains lower salinities

https://doi.org/10.5194/egusphere-2023-1403
Preprint. Discussion started: 28 June 2023
© Author(s) 2023. CC BY 4.0 License.

nearshore on the continental shelf and relatively higher salinities > 30 pss offshore. Therefore, the salinity range captured by in-situ observations only collocated with one satellite product/GLORYS12V1 typically includes a larger range of salinities (with more SSS values <30) than that captured by in-situ observations collocated with all products. Hence, the correlation coefficients of almost all products are larger when considering all in-situ observations collocated with that product due to the larger range in SSS than when considering only in-situ observations collocated with all products.

Whilst GLORYS12V1 appears to correlate well with in-situ data when considering all its collocations ($r > 0.79$ over 2015-2020 and $r>0.78$ over 2011-2020), the correlation deteriorates when only considering observations where all satellite products have a collocation ($r < 0.35$ over 2015-2020 and $r < 0.63$ over 2011-2020). This same pattern is visible in all other reanalysis products considered. This decrease in correlation indicates that the reanalyses manage to replicate the large-scale horizontal gradient in SSS (between the fresh plume on the shelf and the more saline water that sits off the shelf, under sea ice) but are not capable of representing the spatial variability at lower SSS values and hence of finer scale river plume dynamics. Reanalysis RMSDs from in-situ data are also all larger than those of any satellite product. The lower RMSDs and stronger correlation coefficients of all satellite products compared to reanalyses highlight the value satellite SSS products bring to Arctic-based process studies.

https://doi.org/10.5194/egusphere-2023-1403
Preprint. Discussion started: 28 June 2023
© Author(s) 2023. CC BY 4.0 License.

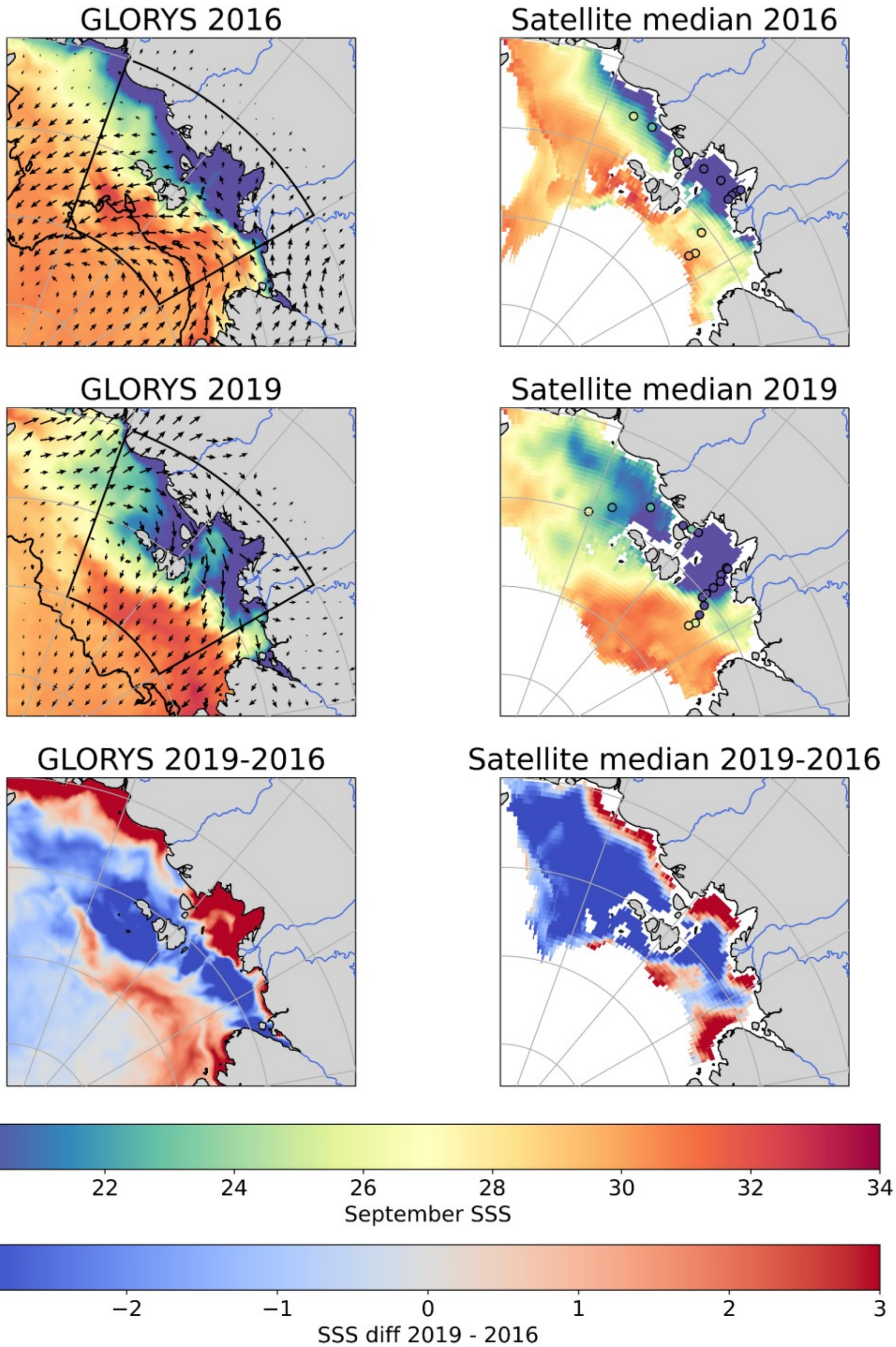

255 **Figure 2 : Laptev Sea sea surface salinity** ***field in September (9) 2016 (top) and 2019 (middle) and the difference between 2016 and 2019 (bottom) for the median of 4 satellite products (RSS SMAP, JPL SMAP, LOCEAN SMOS, BEC SMOS) (right) and for the CMEMS GLORYS12V1 reanalysis (left). ERA5 mean wind speed for June-September are overlaid on the GLORYS12V1 SSS field with a box over the region of interest (70-80°N, 120-160°E). The GLORYS12V1 30% sea ice concentration contour is also overlaid as a black line over the GLORYS12V1 SSS field. In-situ data for late September 2016 and early October 2019 are overlaid on satellite median products using the same colour scale.***

There is close agreement between the September SSS pattern in GLORYS12V1 and the median satellite September SSS product in all years compared (Figure 2). The SSS off the continental shelf (> 100 m) or above 75 °N is typically > 28 pss in both years analysed and in both products. SSS generally decreases with proximity to shore, and is lowest near the outflow of the Lena River, around 130 °E, with salinity values as low as 10 pss nearshore. This low salinity area (< 20 pss) extends considerably to the East of the Lena River outflow throughout the southern Laptev Sea and past the New Siberian Islands into the East Siberian Sea, extending to over 160 °E in both years.

The years 2016 and 2019 stand out as having notably anomalous patterns of Laptev SSS, with differences in SSS of over 10 pss from the median satellite product. Both the satellite median product and GLORYS12V1 SSS capture the same pattern of SSS interannual variability as in-situ data from cruises in all years of overlap (2016 and 2019 shown in Fig. 1). In 2016, the freshest salinities are coastally confined and do not travel far off the continental shelf. In 2019, the freshest salinities travel considerably further offshore, and extend over most of the Western Laptev and East Siberian Sea.

Despite the strong overall similarity between gridded products, notable differences are visible between in-situ data and both the satellite median product and GLORYS12V1 SSS. The fresh layer in Figure 2 typically appears to extend further offshore in in-situ data than in GLORYS12V1 or in the satellite median product. However, this difference is likely primarily due to the temporal mis-match between GLORYS12V1 and in-situ data as in-situ data was collected in late September 2016 and early October 2019, but are compared with mean SSS in September. Both GLORYS12V1 and satellite SSS do show the plume extending further offshore by the following month (not shown), supporting this suggestion.

Most of the products used to generate the satellite median (GLORYS12V1, LOCEAN SMOS and both SMAP products) clearly manage to capture a consistent pattern of interannual variability (see Figure A1, Figure A2). However, notably different patterns are observed in the BEC product. All other satellite products analysed here appear to capture the SSS pattern described above for 2016 and 2019. This difference in SSS pattern agrees well with the two modes of SSS variability previously observed in in-situ data and described by other studies in this region (Dmitrenko et al., 2005; Osadchiev et al., 2021). Of the four products considered here, the LOCEAN SMOS Arctic and JPL SMAP products capture particularly consistent patterns of interannual variability, especially given they originate from different satellites and are generated from different processing algorithms. These two products (LOCEAN SMOS and JPL SMAP) are chosen for further use in this study, due to their strong similarity and good correlation values with in-situ data.

There is also a good agreement between the area of open water in GLORYS12V1 (shown as the 30% sea ice concentration) and the area of no retrievals / of open water in the two satellite products. In 2019, the area of open water is particularly large in GLORYS12V1 and in all satellite products, with no regions of notable sea ice (where sea ice concentration > 30%) below

https://doi.org/10.5194/egusphere-2023-1403
Preprint. Discussion started: 28 June 2023
© Author(s) 2023. CC BY 4.0 License.

80°N throughout the Laptev and East Siberian Seas. In 2016, there is more extensive sea ice and few satellite SSS retrievals in the Laptev Sea but a large area of open water in the East Siberian Sea, which extends considerably offshore to over 80 °N.

https://doi.org/10.5194/egusphere-2023-1403
Preprint. Discussion started: 28 June 2023
© Author(s) 2023. CC BY 4.0 License.

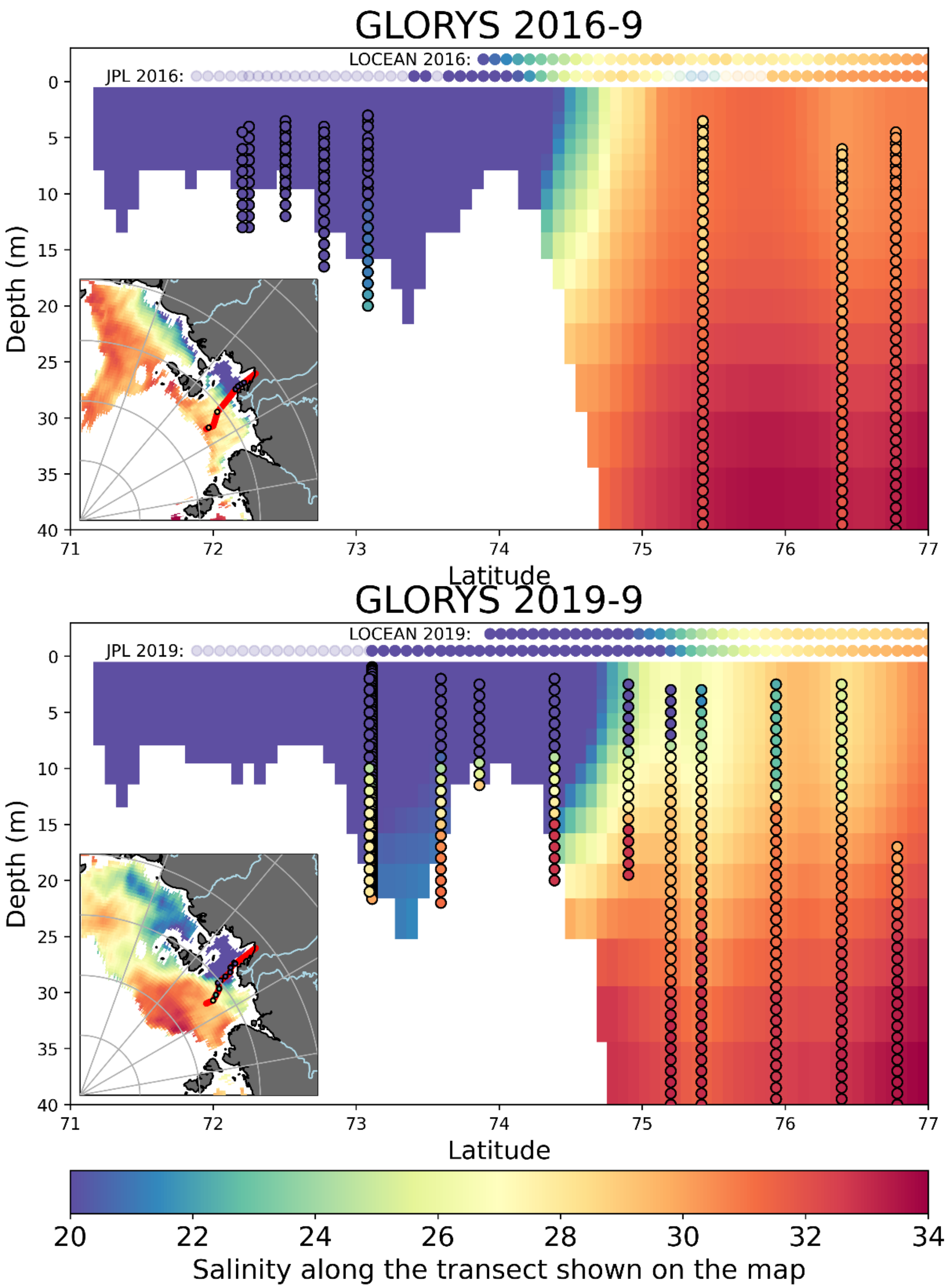

300 **Figure 3** *: GLORYS12V1 SSS vertical transect in 2016 (top) and 2019 (bottom) along red transect interpolated through insitu data (shown in map of JPL SMAP SSS in bottom left for each year) with insitu data overlaid with black rings and satellite data for that transect in JPL SMAP and LOCEAN SMOS SSS shown as a line of points. JPL SMAP data is made semi-transparent where the provided SMAP uncertainty is < 1 pss.*

https://doi.org/10.5194/egusphere-2023-1403
Preprint. Discussion started: 28 June 2023
© Author(s) 2023. CC BY 4.0 License.

GLORYS12V1 features a well-mixed plume in the shallowest regions of the shelf in 2016 and 2019 (Figure 3), and in almost all other years considered. Hence, it agrees well with in-situ data in regions and years where the plume is well-mixed nearshore (e.g. 2016 shown above and 1994 and 2000 not shown) but fails to represent years with a stratified plume nearshore (e.g. 2019 shown above and 2008, 2011 not shown). In all years examined, in-situ data shows the fresh layer (< 15 pss) is relatively shallow and only extends to between 5 and 10m, shallower than Kara due to weaker tidal mixing (Osadchiev et al., 2021).

In 2019, some differences in surface plume extent are visible between GLORYS12V1 and in-situ data. Some of these differences may be due to spatio-temporal mismatch of September monthly 1/12 degree data with point in-situ data (in late September/early October), as vertical stratification is very seasonally and regionally variable (and bathymetrically controlled) in this region (Janout et al., 2020). However, both satellite products more closely resemble the extended plume visible in in-situ data than GLORYS12V1.

In addition, previous studies show considerable interannual variability in the lowest values of SSS at the outflow of the Lena River. Whilst in some years, there are only very small regions of SSS below 20 pss (2014), in other years, notable regions of SSS as low as 6 pss have been observed (in 2013) (Janout et al., 2020). Within GLORYS12V1, the shallow surface layer is consistently more saline (between 15-20 pss) than in-situ data and salinities below 20 pss are typically very confined to the shelf. Although there are few satellite SSS retrievals near the coast (due to land contamination), nearshore SSS are notably lower and quite variable (10-20 pss) in LOCEAN SMOS and JPL SMAP and more consistent with in-situ data. Overall, within shallow shelf regions (< 20 m), the more saline surface waters, fresher bottom waters and less extensive surface plumes suggest GLORYS12V1 is too well-mixed compared to in-situ data. This is reinforced by the weak tidal influence in this region and as there is rarely sufficient wind-driven mixing to break up such strong stratification (Fofonova et al., 2014; Hölemann et al., 2011; Janout and Lenn, 2014; Shakhova et al., 2014).

Salinity stratification on the shelf is much stronger than that of temperature and is by far the dominant control on density in this region (Osadchiev et al., 2021). Sea surface temperature, and in turn stratification in temperature also vary considerably over the course of September, so a higher temporal resolution analysis would be needed for investigating temperature stratification dynamics. Therefore, this study focuses on salinity stratification in this region, which is more consistent over the course of September, and more appropriately represented by the monthly data used for analysis in this study.

3.2 3 Impact of variability in wind forcing on SSS

The mean atmospheric circulation pattern is represented in Figure 4, calculated as the mean surface stress over the box defined in Figure 2. Values are notably different in 2016 and 2019 (Figure 2). In 2016, there is predominantly cyclonic circulation,

https://doi.org/10.5194/egusphere-2023-1403
Preprint. Discussion started: 28 June 2023
© Author(s) 2023. CC BY 4.0 License.

with strong Eastward winds dominant over the Laptev Sea shelf, and Northward winds present over the region of the Laptev Sea just off the continental shelf. In 2019, there is predominantly anticyclonic circulation with North-westward winds dominant over the Laptev Sea shelf. The anticyclonic circulation visible in 2019 more closely resembles the mean circulation pattern visible (in Figure 1) over 2011-2020.

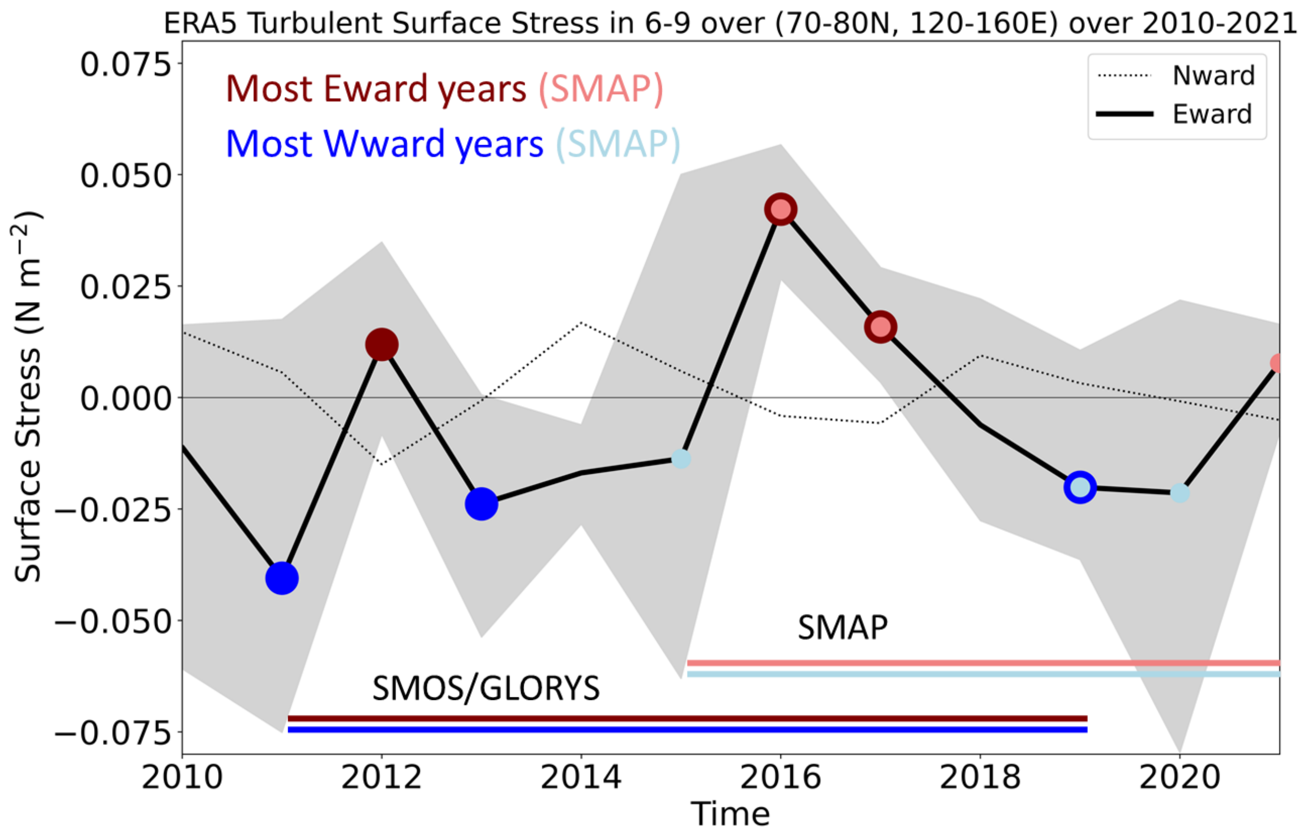

Figure 4 : Timeseries of the mean June to September ERA5 eastward (black solid) and northward (black dashed) turbulent surface stress over 70-80 North and 120-160 East. Overlaid are dots indicating the most Eastward (red dots) and Westward (blue dots) years chosen for analysis for both the longer SMOS/GLORYS12V1 timeseries (darker red and blue dots) and the shorter SMAP timeseries (lighter red and blue dots) . The range of the maximum and minimum eastward turbulent surface stress between June and September is shaded in grey.

The magnitude of variability in mean eastward turbulent surface stress (± 0.05 N m^{-2}) across the entire timeseries is notably larger than that of northward turbulent surface stress, which remained within ± 0.02 N m^{-2}. The years of highest eastward turbulent wind stress are 2012, 2016, 2017 over the SMOS timeseries and 2016, 2017 and 2021 over the SMAP timeseries. The years of strongest westward turbulent wind stress are 2011, 2013 and 2019 over the SMOS timeseries and 2015, 2019 and 2020 over the SMAP timeseries. In years where the mean eastward turbulent surface stress is negative (denoting predominant westward turbulent surface stress), there is considerably more within-year variability (typically > 0.05 N m^{-2} in eastward turbulent surface stress in the months spanning June to September (denoted by the grey overlay in Figure 4).

https://doi.org/10.5194/egusphere-2023-1403
Preprint. Discussion started: 28 June 2023
© Author(s) 2023. CC BY 4.0 License.

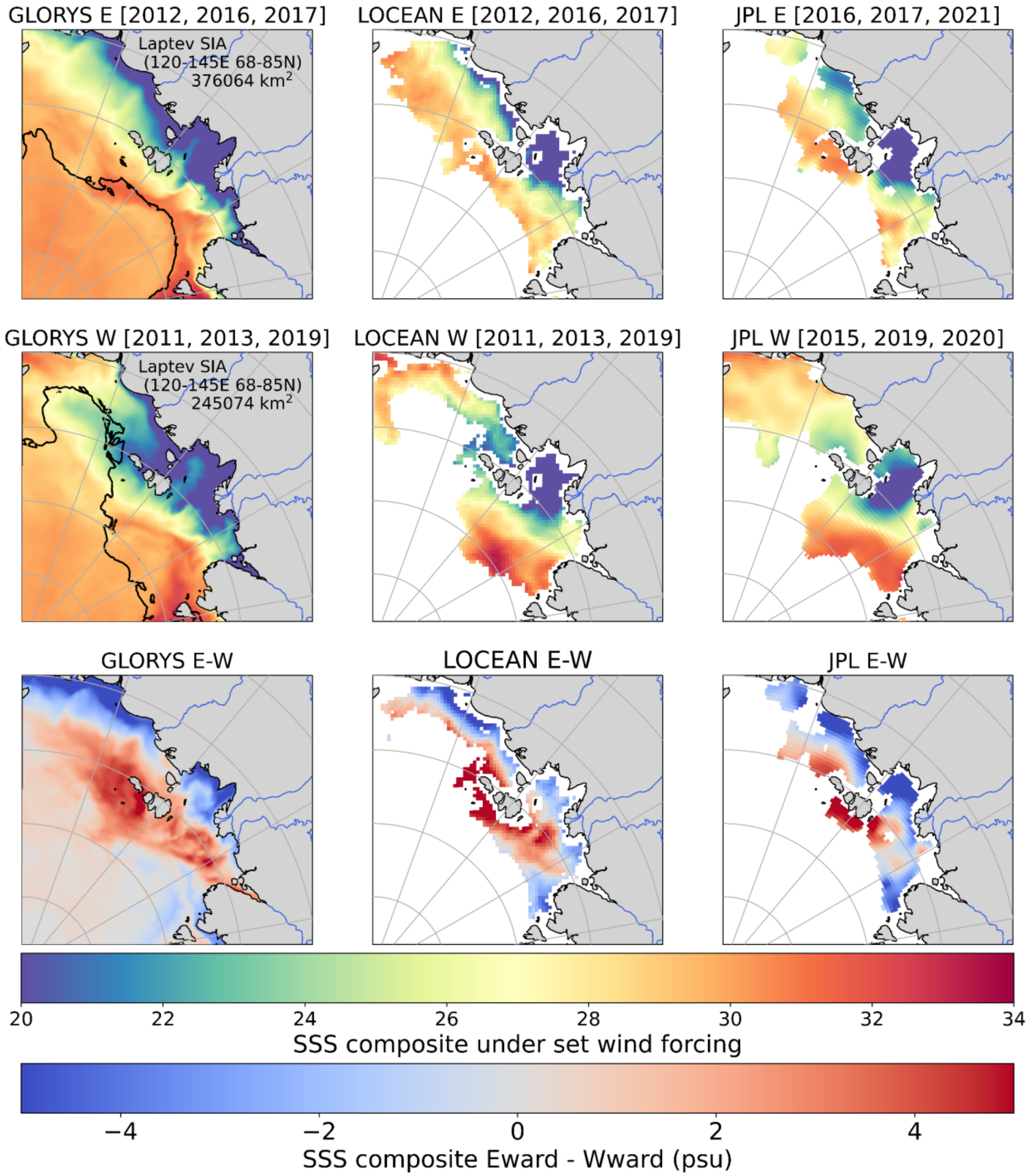

355 **Figure 5 :** ***Eastward (E, top row) and westward (W, middle row) composites calculated from the identified three most eastward and westward years for (left to right) GLORYS12V1 SSS, LOCEAN SMOS and JPL SMAP. The difference composite (eastward – westward) for each product is shown on the bottom row. The GLORYS12V1 mean 30% sea ice concentration contour and mean GLORYS12V1 sea ice area (SIA) in the Laptev Sea (120-140, 68-85N) for eastward and westward years is overlaid on the respective composite plots.***

https://doi.org/10.5194/egusphere-2023-1403
Preprint. Discussion started: 28 June 2023
© Author(s) 2023. CC BY 4.0 License.

The eastward/westward composites of all three SSS products agree strongly, regardless of the differing years chosen for analysis (Figure 5). The composite analysis clearly highlights the differing pattern of SSS under positive (eastward) and negative (westward) zonal wind. The eastward composite closely resembles the 2016 SSS pattern visible in Figure 2, and the westward composite closely resembles the 2019 SSS pattern. This strong resemblance between particularly anomalous individual years and the zonal wind composite plots supports that the zonal wind is the dominant driver of variability in this region. Years with strong westward wind have considerable offshore transport, and northward spreading of the plume, denoted by the presence of anomalous fresh water in the Northern Laptev Sea and relatively higher salinity water in the East Siberian Sea. Alternatively, years of eastward wind are associated with onshore and alongshore transport, and a coastally confined plume, denoted by more saline waters in the Northern Laptev Sea and fresher waters in the Southern Laptev and East Siberian Seas.

The composite difference plots provide a more clear visualization of the North/South (offshore/nearshore) dipole in freshwater transport visible under eastward/westward wind forcing. The strong agreement between all three products strengthens the weighting of this finding, particularly as the difference plots appear to agree even more closely than the individual eastward/westward composites. This agreement suggests that although the three products have different mean SSS states, they capture very similar patterns of variability.

There is a notable difference in SIA in years of westward and eastward wind forcing in both GLORYS12V1 and the satellite data (indicated by the absence of SSS data). Under westward wind forcing, the Laptev SIA is smaller in the Laptev Sea (245074 km^2) and the 30% sea ice concentration contour is nearer shore in the East Siberian Sea. The opposite is true under eastward wind forcing, with a larger SIA in the Laptev Sea (376064 km^2) and the 30% sea ice concentration contour further offshore in the East Siberian Sea.

https://doi.org/10.5194/egusphere-2023-1403
Preprint. Discussion started: 28 June 2023
© Author(s) 2023. CC BY 4.0 License.

3.4 Impact of variability in wind forcing on SST

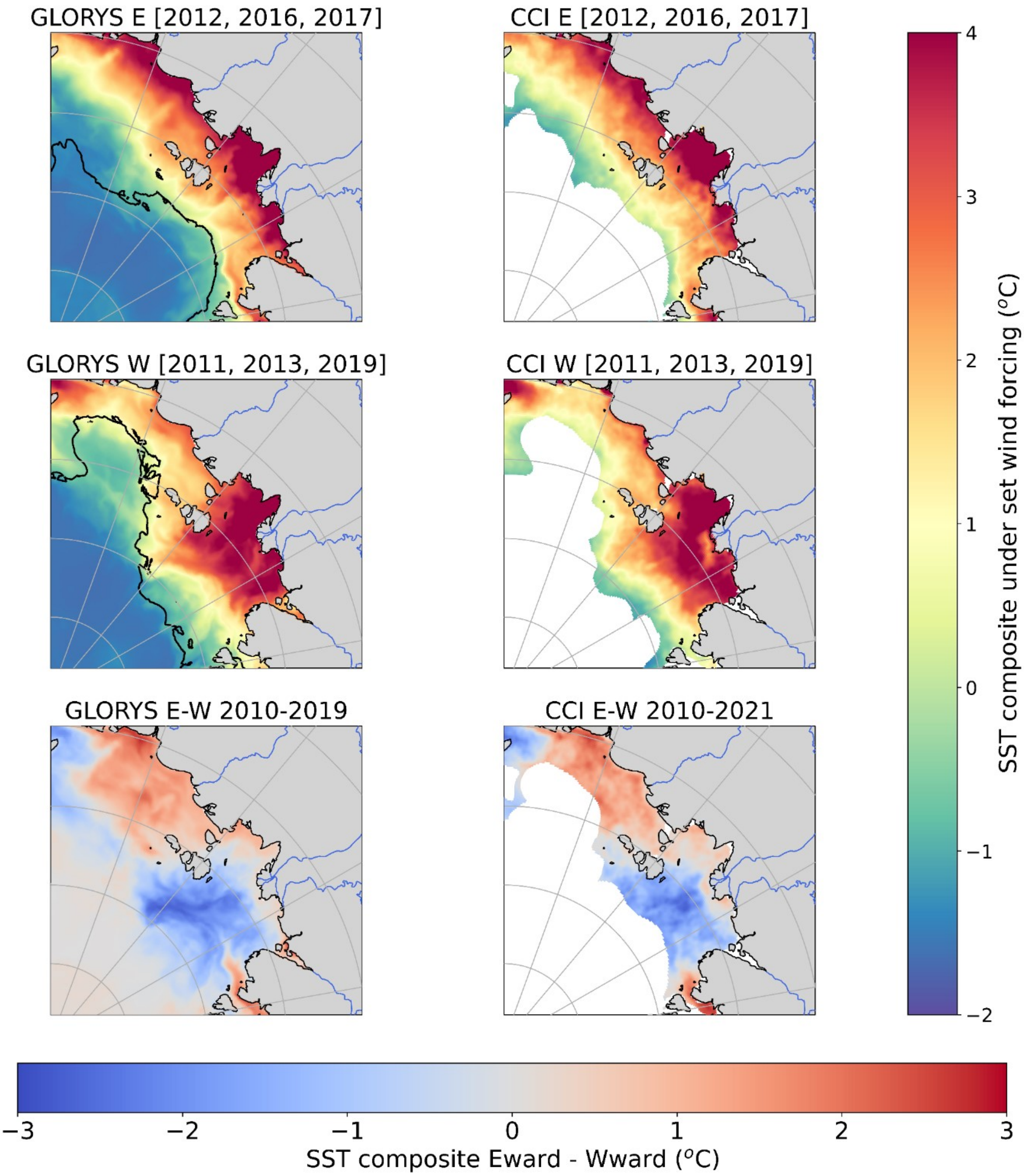

385 **Figure 6 :** ***Eastward (E, top row) and westward (W, middle row) composites calculated from the identified three most eastward and westward years for (left to right) GLORYS12V1 SST and L4 CCI SST (masked by 30% sea ice concentration). The difference composite (eastward – westward) for each product is shown on the bottom row. The mean 30% sea ice concentration contour for eastward and westward years is used to mask L4 CCI data and is overlaid in GLORYS12V1 in black on both eastward and westward composite plots.***

https://doi.org/10.5194/egusphere-2023-1403
Preprint. Discussion started: 28 June 2023
© Author(s) 2023. CC BY 4.0 License.

Similar to Figure 5, Figure 6 represents the eastward and westward composites of GLORYS12V1 and ESA CCI SST (Figure 6). Temperatures < 1°C are typically present off the continental shelf in both composites (and all years analysed), with a rapid transition in temperature present at the 30% sea ice concentration margin (Figure 6). On the shelf, temperatures are typically warmer (> 1°C) and riverine plume is typically > 2°C, with large regions in excess of 4°C.

The eastward/westward composites of both products agree very well and suggest notable differences in SST pattern under differing zonal wind forcing. Under eastward wind forcing, both GLORYS12V1 and CCI SST composites show that warm SST anomalies are confined to the southern Laptev Sea and travel alongshore towards the East Siberian Sea. This eastward wind state is coincident with a larger SIA in the Laptev Sea and a 30% sea ice concentration contour nearer shore in the East Siberian Sea. Under westward wind forcing, both SST composites show warm SST anomalies are mostly advected offshore to the Northern Laptev Sea. The westward wind state is coincident with lower SIA in the Laptev Sea and a 30% sea ice concentration contour further from shore in the East Siberian Sea. A dipole composite pattern is also visible in the SST difference composite, as is visible in the SSS difference composite. However, the difference composite between eastward and westward wind states presents in an East/West direction rather than a North/South direction.

4 Discussion

4.1 Variability in runoff

No clear relationship is observed between the magnitude of cumulative spring/summer river discharge and the pattern of Laptev SSS. It might be expected that years with the largest magnitude of cumulative summer / annual river discharge would have the largest fresh surface layer (< 20 pss) and freshwater content as has previously been suggested (Umbert et al., 2021). However, if anything the opposite pattern appears true in most of the years used for the composite analysis. Whilst 2016 and 2017 both have some of the highest September cumulative runoff of any year considered (Umbert et al., 2021), they both have particularly small areal fresh surface layer. In addition, 2011 has one of the smallest September cumulative runoffs but one of largest fresh surface layers (Figure A1). However many years do not follow either pattern, as both 2013 and 2015 have relatively large fresh surface layers and medium and high spring runoff peaks (Umbert et al., 2021). This inconsistent response suggests cumulative runoff is not a major driver of SSS pattern, as previously suggested (Osadchiev et al., 2021).

In addition, GLORYS12V1 doesn't have interannually varying river runoff but manages to represent the SSS pattern well as compared to satellite SSS, suggesting variability in river runoff is not needed to accurately replicate interannual variability in GLORYS12V1 SSS. The strong resemblance between interannual variability in GLORYS12V1 and the satellite products suggests interannual variability in Lena River discharge has little influence on variability in Laptev SSS.

https://doi.org/10.5194/egusphere-2023-1403
Preprint. Discussion started: 28 June 2023
© Author(s) 2023. CC BY 4.0 License.

4.2 Wind variability as driver of SSS variability

Previous studies using sparse in-situ data have suggested wind forcing appears to drive some variability in freshwater transport (Dmitrenko et al., 2005; Osadchiev et al., 2021). Satellite SSS data shown here provides a complete picture of SSS variability and confirms what has previously only been suggested from in-situ data: that zonal wind forcing is the dominant driver of Laptev SSS. Satellite SSS data also provides a clear, complete visualization of differences in freshwater transport throughout the sea ice free Laptev and East Siberian seas under different wind regimes, augmenting the scattered view available from in-situ data. Westward wind drives considerable offshore transport, and northward spreading of the plume toward the Northern Laptev Sea. Conversely, eastward wind is found to drive alongshore transport, resulting in a coastally confined river plume, denoted by more saline waters in the Northern Laptev Sea and fresher waters in the Southern East Siberian Sea. Given the different eastward and westward years chosen for composite analysis for SMOS and SMAP, the agreement in eastward (/westward) SSS composites between JPL SMAP and LOCEAN SMOS products solidifies this finding.

The composite analysis highlights the dominance of the zonal wind over the meridional wind in driving SSS patterns. Within regions with particularly shallow shelf bathymetry, such as in the South Laptev Sea, the Ekman current has been suggested to almost completely align with wind direction or to be transported ~60° to the right (Dmitrenko et al., 2005; Kubryakov et al., 2016; Zatsepin et al., 2015). The strong dominance of the zonal over meridional wind component observed here (in driving the fresh surface layer SE / NW) supports that full Ekman spiral doesn't manifest and that the dominant direction of transport is to the right of the wind but not fully perpendicular to it.

Meridional wind stress also does appear to play a role in plume transport but only in the absence of strong zonal wind stress. This has previously been shown to be true for both 2014 (Janout et al., 2020) and 2018 (Tarasenko et al., 2021), where the wind is primarily northwestward and fresh water is transported directly offshore. Both LOCEAN SMOS and JPL SMAP support this.

There has historically been some debate as to the role of the AOI in controlling SSS variability, both locally (Bauch et al., 2010; Janout et al., 2015; Steele and Ermold, 2004), and on a full Arctic basin scale (Morison et al., 2012; Rabe et al., 2014). The mean eastward zonal surface stress in this region is found to be strongly correlated to the mean Arctic Oscillation Index (AOI) over June-September over the full GLORYS12V1 timeseries (r=0.49), and this correlation is particularly strong over the SMOS satellite period (r>0.67).

Very similar spatial patterns are found when calculating composites from the three years of maximum and minimum (June-September) AOI as when calculating composites from years of maximum and minimum (June-September) ERA5 zonal surface stress (not shown). The similar spatial patterns highlight that local wind variability in this region is predominantly governed

https://doi.org/10.5194/egusphere-2023-1403
Preprint. Discussion started: 28 June 2023
© Author(s) 2023. CC BY 4.0 License.

by large-scale dynamics over this period. The considerable variability in correlation strength (depending on time period analysed) suggests there may be some decadal variability in the extent to which the AOI controls local wind forcing in this region. In addition, the decline in summer sea ice will increase the area of atmospheric influence and in turn could alter how strongly coupled the AOI is to local wind forcing in this region.

4.3 Vertical distribution of plume

Nearshore in-situ data suggests that the two modes of SSS variability, visible under eastward/westward wind forcing appear to be related to very different stratification dynamics (Figure 3). In 2016, in-situ and GLORYS12V1 SSS agree particularly well and show a well-mixed very fresh plume nearshore (Figure 3), likely driven by the strong consistent onshore Ekman transport driving downwelling (Osadchiev et al., 2021). This year (2016) stood out as having a particularly well mixed plume compared to all other in-situ data in this region, the extent of which had not previously been observed (Janout et al., 2020) . A similar dynamic appears to be visible in 1994, where strong eastward wind stress is coincident with a coastally confined and well-mixed plume (not shown but visible in in-situ data and GLORYS12V1 SSS and SST).

Conversely, in-situ data showed a strongly stratified fresh layer in 2008, 2011 and 2019, even in shallow regions on the shelf (Osadchiev et al., 2021), which is poorly represented nearshore in GLORYS12V1 (Figure 3). The strong stratification on the shelf, visible in in-situ data in these years, suggests that the fresh layer is more strongly stratified in years with considerable northward spreading. This phenomenon appeared true in 1994 and 2016, where strong onshore Ekman transport appeared to drive the well-mixed plume observed. Hence, despite that the shallow shelf is below the calculated Ekman depth for this region (37 m) (Baumann et al., 2018; Tarasenko et al., 2021), Ekman transport clearly plays a role in controlling vertical stratification, at least in years where eastward wind stress drives onshore transport and mixing / downwelling (Lentz and Helfrich, 2002). However, it is also possible that the magnitude of river discharge is a dominant control on the vertical distribution of SSS, given the surface freshwater content does not appear to directly vary with cumulative discharge magnitude (Umbert et al., 2021).

This hypothesis was not tested as the constant well-mixed plume nearshore suggests GLORYS12V1 is not capable of fully representing plume stratification dynamics in this complex environment. Other model output was considered for use (including CMEMS TOPAZ, GLORYS2V4, ORAS5, GloSea5/FOAM, CGLORS), but all models considered either had insufficient vertical levels to accurately resolve the shallow shelf (TOPAZ) or suggested the shallow shelf to be well-mixed in all years considered. The challenge of accurately representing mixing/stratification dynamics in Arctic shallow shelf seas has been widely documented (Janout et al., 2020; Hordoir et al., 2022). Given the large number of vertical layers present in GLORYS12V1, even on the shallow shelf, it is likely poor representation of vertical stratification is due to model physics / parameterization of vertical mixing rather than due to insufficient vertical layers to be able to realistically represent the plume.

https://doi.org/10.5194/egusphere-2023-1403
Preprint. Discussion started: 28 June 2023
© Author(s) 2023. CC BY 4.0 License.

Even in years with a mostly well-mixed plume (EG 2016), in-situ data typically shows a more saline layer at depth in certain regions on the shelf, which is almost never captured by GLORYS12V1. The challenge of accurately modelling stratification in Arctic shallow shelf seas and the very limited availability of in-situ data on the shelf prevents a more in-depth analysis of the representation of vertical plume structure within GLORYS12V1.

4.4 Sea surface temperature (SST) / sea ice concentration variability

SST has been shown to be a useful indicator of plume location in this region (Dmitrenko et al., 2005; Osadchiev et al., 2021; Tarasenko et al., 2021). During the summer, Lena river water is typically at around 16°C before entering the Laptev Sea, which is much warmer than the typical SST below sea ice of below 0°C (Juhls et al., 2020). This sets up the gradient in SST that is clearly visible over the Laptev Sea, with temperatures below 0°C off the continental shelf and below sea ice and temperatures above 4°C present over much of the shelf. Similar results have previously been shown from in-situ data, with offshore SSTs typically below 0 °C and SSTs near the mouth of the Lena River typically over 3 °C and up to 10 °C in the last 2 decades (Osadchiev et al., 2021). This represents a significant increase in September near-shore SSTs over the last several decades (Kraineva and Golubeva, 2022; Polyakov et al., 2005).

Many studies have considered the dominant drivers of SSS interannual variability and of the seasonal and decadal variability in SST, but few have considered whether SSS and SST co-vary with distance from the mouth of the Lena and in turn what drives interannual variability in SST in this region. The composite analysis shows that zonal wind component is a key driver of interannual variability in SST as well as of SSS. This finding highlights that correspondence between SSS and SST is not only driven by their common source but also by their common driver of interannual variability. The strong correspondence between eastward/westward SSS and SST composites on the shallow Laptev shelf is unsurprising given that warm and fresh Lena River water dominates oceanic properties in this region.

However, whilst the eastward/westward composites appear similar, considerable differences are observed between the SSS and SST composite difference plots. The SSS composite (eastward-westward) difference plots suggest a North/South dipole where eastward forcing appears to drive onshore / southeastward transport of fresh SSS anomalies and westward wind forcing drives offshore / northward transport of fresh SSS anomalies. Conversely, the SST composite (eastward-westward) difference plots show more of an East/West dipole where eastward surface stress drives eastward transport of warm SST anomalies and westward surface stress drives northwestward transport of warm SST anomalies. These differences in composite difference plots likely occur due to feedback cycles between SST, SIA, SSS and albedo.

Hence, whilst the zonal wind clearly plays a key role in controlling both SSS and SST patterns, the differences between SSS and SST composite difference plots highlight that this warm and fresh water is exposed to very different thermal and freshwater

https://doi.org/10.5194/egusphere-2023-1403
Preprint. Discussion started: 28 June 2023
© Author(s) 2023. CC BY 4.0 License.

forcing after entering the Laptev Sea. Comparing the responses of SSS and SST provides unique insight into understanding the contribution of the zonal wind in distributing warm riverine anomalies and the contribution of summer heating to the September SST pattern.

Regardless of differences in SSS and SST composite difference plots, the zonal wind clearly controls the initial plume propagation. Under eastward wind forcing, it transports the fresh, warm plume along the coast to the East Siberian Sea, and otherwise, under westward wind forcing, it transports the plume offshore to the Northern Laptev Sea. SST is a dominant control on the spatial distribution of September sea ice concentration in this region so the initial transport of this plume drives sea ice melt in that region. This relationship is highlighted by the very strong correlation (r=0.91) between mean SST over the Laptev Sea and SIA in September. The strong correlation found between river-water fraction and melt-water fraction supports that this relationship is causal rather than coincidental (Bauch et al., 2013). Despite this strong correspondence, the initial heat brought by river runoff is only suggested to contribute ~10% to sea ice breakup in early spring (Dean et al., 1994). However, the initial loss of sea ice near the river mouth and the dark-coloured water that replaces it (high in dissolved and suspended particulate matter) alters surface albedo and increases heat absorption creating a strong positive feedback (Bauch et al., 2013; Park et al., 2020). As SST is cooler than atmospheric air temperature in summer, SSTs will continue to warm until atmospheric temperatures start to cool in autumn (Janout et al., 2016). The strongly stratified summer halocline also increases stability of the water column, making summer heating more effective (Osadchiev et al., 2021). Whilst warm summer air temperatures will drive a warming of SST in open water regions, freshwater input from precipitation has a negligible impact on SSS and sea ice melt only plays a small role in altering summer SSS (Dubinina et al., 2017). These differences drive the observed differences in composite difference plots. The SSS composite difference plots represent just the direct response of SSS to the zonal wind (offshore/nearshore). The SST composite difference plots also highlight the importance of the SST/SIA positive feedback: whereby warm river runoff drives sea ice melt, in turn increasing the area of shallow open water exposed to the warm atmosphere, and further driving SST warming in newly open water regions. It is worth noting that the similarity between SSS and SST eastward/westward composites highlights the importance of the zonal wind in modulating this SST/SIA warming positive feedback.

The considerable difference in spatial pattern of sea ice concentration under eastward and westward wind forcing and the relationship between SST and SIA suggests zonal wind is not only a key driver of variability in SSS and SST but also of Laptev SIA. There have previously been Arctic-wise studies that have suggested that the summer AOI is a good predictor of September sea ice concentration (Ogi et al., 2016), but the same has not yet been suggested locally in the Laptev Sea. The consistency of SST composites calculated in this study from years of strong eastward (/westward) turbulent surface stress with that of strongly positive (/negative) AOI years supports that large scale circulation appears to be the dominant driver of variability in this region.

https://doi.org/10.5194/egusphere-2023-1403
Preprint. Discussion started: 28 June 2023
© Author(s) 2023. CC BY 4.0 License.

Previous work in this region has also suggested that variability in SSS is unrelated to sea ice dynamics (Osadchiev et al., 2021). However, the composite analysis here clearly shows that variability in zonal wind stress does play a role in controlling SST, and therefore in turn sea ice concentration and SIA. Attributing variability in SST and in turn sea ice concentration/SIA to zonal wind stress is complex due to the SST/SIA warming positive feedback described above and the strong decline in SIA visible in the Laptev (Kraineva and Golubeva, 2022).

However, the spatial pattern of GLORYS12V1 eastward and westward SST composites is consistent regardless of time period chosen (the full GLORYS12V1 time period, the LOCEAN SMOS time period or the JPL SMAP time period), suggesting this relationship doesn't only exist due to the SIA trend (IE if years of westward/eastward forcing are present earlier/later in the timeseries). In addition, the spatial pattern of variability visible in both SST composite difference plots is notably different from the long-term pattern of SST warming (between 1993-2002 and 2010-2019 in GLORYS12V1), which suggests a pattern of more rapid warming distributed across the continental shelf. Both the consistency of SST composites shown and the difference in spatial pattern of SST support that wind stress is a control on SST and in turn September SIA. Further work is needed to investigate if variability in SSS and SST impact later sea ice formation as well as September SIA.

4.5 Implications with climate change

The increase in riverine heat has already contributed to a regional loss of sea ice, and it has been suggested that warming river discharge is a key control on basin-wide SIA (Dong et al., 2022; Park et al., 2020). It is also clear that the increase in river runoff will increase the freshwater content of the Laptev Sea and have implications for local and Arctic-wide stratification dynamics as well as for local biogeochemistry. However, the dominance of zonal wind as a key driver of SSS and SST interannual variability suggests that understanding variability in wind stress and if it is likely to change is the key to predicting future freshwater transport from the Eurasian shelf seas.

This is all the more relevant as the dominance of wind stress variability is only likely to increase with the loss of sea ice cover. Prior to the mid-2000s, the Lena plume typically remained strongly-stratified and confined to the Laptev Sea shelf, constrained by the extensive sea ice cover and small region of atmospheric influence (Janout et al., 2020). The loss of sea ice cover in the Laptev Sea is enlarging the area in contact with the atmosphere and increasing the time of atmosphere-ocean exposure.
The strong influence of the AOI on local wind stress in this region, and the increase in correlation strength over the more recent time period, highlights the need to investigate how large scale atmospheric circulation will change over the Arctic to understand future changes in Laptev Sea freshwater transport. This relationship is only likely to become stronger given the AOI is suggested to have increased in variability in recent decades (Armitage et al., 2018; Morison et al., 2021), and as future sea ice loss will only strengthen coupling between large scale and local wind dynamics. These changes have already and will likely continue to expand the region of potential riverine freshwater influence (Janout et al., 2020; Johnson and Polyakov, 2001;

https://doi.org/10.5194/egusphere-2023-1403
Preprint. Discussion started: 28 June 2023
© Author(s) 2023. CC BY 4.0 License.

Zhuk and Kubryakov, 2021) and in turn have the potential to speed up transport between the shelf seas and central Arctic (Charette et al., 2020).

However, the impact this will have on the wider Arctic will strongly dependent on changes in stratification dynamics in the Laptev Sea. Whilst it is likely that stratification dynamics will change as the region of potential freshwater influence expands, it remains uncertain what the dominant drivers of this change will be and in turn how this change will manifest. On the one hand, having a larger open-water region exposed to wind-driven mixing for longer periods could deepen stratification, increasing the tendency of a well-mixed plume (Janout et al., 2020). This appeared to occur in 2016 and seems likely under strong eastward wind forcing, where the fresh water is transported eastwards, driving downwelling and mixing and creating a coastally confined well-mixed plume. Alternatively, the increase in river runoff to the Arctic could strengthen surface stratification (Nicolì et al., 2020; Nummelin et al., 2016) and increasing tendency of a very shallow plume that extends out northwards towards the central Arctic. It is also possible that the likelihood of both of these alternating states could become more frequent, with the increased influence of wind variability with the loss of sea ice cover (Janout and Lenn, 2014). Changes in stratification will be strongly coupled to changes in sea ice dynamics, not only in summer but also year round, and will have implications for the timing, magnitude and region of water mass formation / transformation in the Laptev (Preußer et al., 2019). Untangling all these compounding changes remains a challenge and will only be solved by a unified approach bringing together a combination of different data products and types including in-situ data, satellite data and model output. The long satellite SSS timeseries has, and with the launch of the Copernicus Imaging Microwave Radiometer (CIMR), will continue to be a valuable asset in understanding Arctic wide freshwater transport. Understanding these processes will be further aided by the launch of higher resolution satellites for mapping sea surface geostrophic (and total) velocity, including the Surface Water and Ocean Topography (SWOT), SeaSTAR, Harmony and ODYSEA (Gommenginger et al., 2019; Morrow et al., 2019; Suess et al., 2022; Lee et al., 2023).

5 Conclusions

Satellite SSS agrees well with in-situ data and provides notable improvement compared to GLORYS12V1 SSS and the other reanalysis products considered in capturing patterns and variability observed by in-situ SSS data. Hence, satellite SSS provides a useful tool to strengthen our current understanding of Laptev Sea and wider Arctic SSS dynamics, particularly in regions with strong SSS gradients. Comparison between satellite and in-situ data in this region highlights the need for more near-surface in-situ data for validation in this region, particularly nearshore over the lowest salinities. The current lack of nearshore low salinity in-situ data limits the confidence in and ability to validate satellite data over regions of very low salinities (< 20 pss) and limits our understanding of vertical stratification over the shelf, particularly given its high spatial and temporal variability.

https://doi.org/10.5194/egusphere-2023-1403
Preprint. Discussion started: 28 June 2023
© Author(s) 2023. CC BY 4.0 License.

Satellite SSS data confirms what in-situ data has previously suggested: that the zonal wind is the dominant driver of offshore/onshore Lena river plume transport, with strong consensus in SSS patterns under eastward and westward wind regimes in GLORYS12V1, LOCEAN SMOS and JPL SMAP. The zonal wind also played a key role in driving of SST variability and appeared to drive both spatial variability in sea ice concentration across the Laptev/East Siberian Seas and variability in Laptev SIA. The differences in spatial patterns of SSS and SST under eastward/westward wind forcing highlight the importance of the zonal wind for dispersing riverine heat and in turn controlling the SST/SIA positive feedback, which plays a considerable role in driving further SST warming in shallow open water regions. The dominance of local wind stress as a driver of salinity and temperature variability, and its strong correlation with the AOI and large-scale atmospheric circulation, highlights the need to understand how local and large-scale wind stress has and will change as the Arctic warms in order to predict changes in freshwater storage and transport from the Eurasian shelf seas. The interconnected nature of SSS, SST and sea ice concentration in this region highlights the challenge but also the need to understand this region as a system rather than trying to understand drivers of individual components in isolation. This will prove vital to be able to predict how the conflicting changes in this region will impact both this region and wider Arctic sea ice dynamics and freshwater transport.

https://doi.org/10.5194/egusphere-2023-1403
Preprint. Discussion started: 28 June 2023
© Author(s) 2023. CC BY 4.0 License.

Appendix

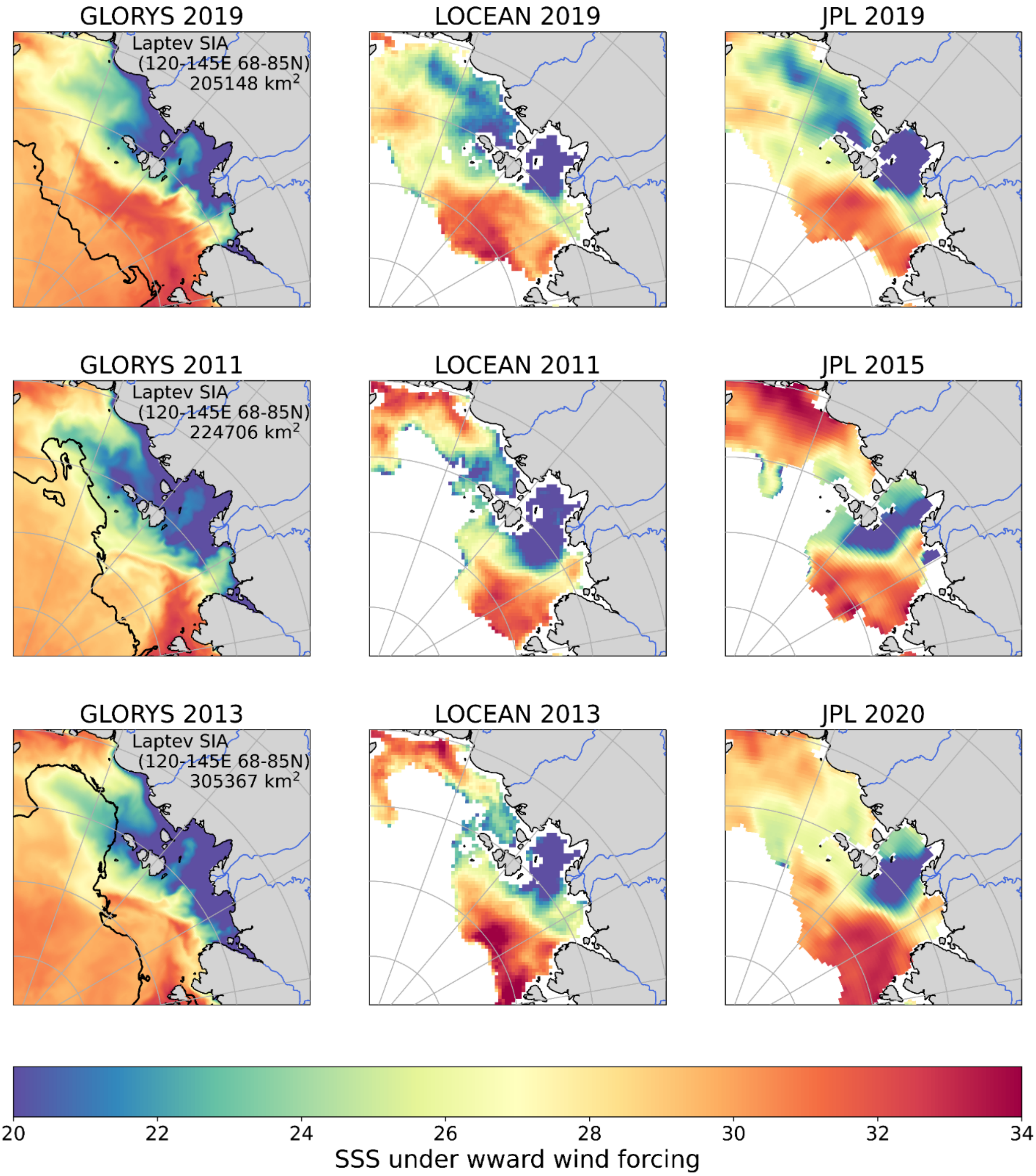

635 **Figure A1 :** *Years of westward wind forcing for all years used to calculate westward composites for (left to right) GLORYS12V1 SSS and LOCEAN SMOS (2019, 2011, 2013) and for JPL SMAP (2019, 2015, 2020). The GLORYS12V1 mean 30% sea ice concentration contour and mean GLORYS12V1 sea ice area (SIA) in the Laptev Sea (120-140, 68-85N) for each year shown is overlaid on that year's plot.*

https://doi.org/10.5194/egusphere-2023-1403
Preprint. Discussion started: 28 June 2023
© Author(s) 2023. CC BY 4.0 License.

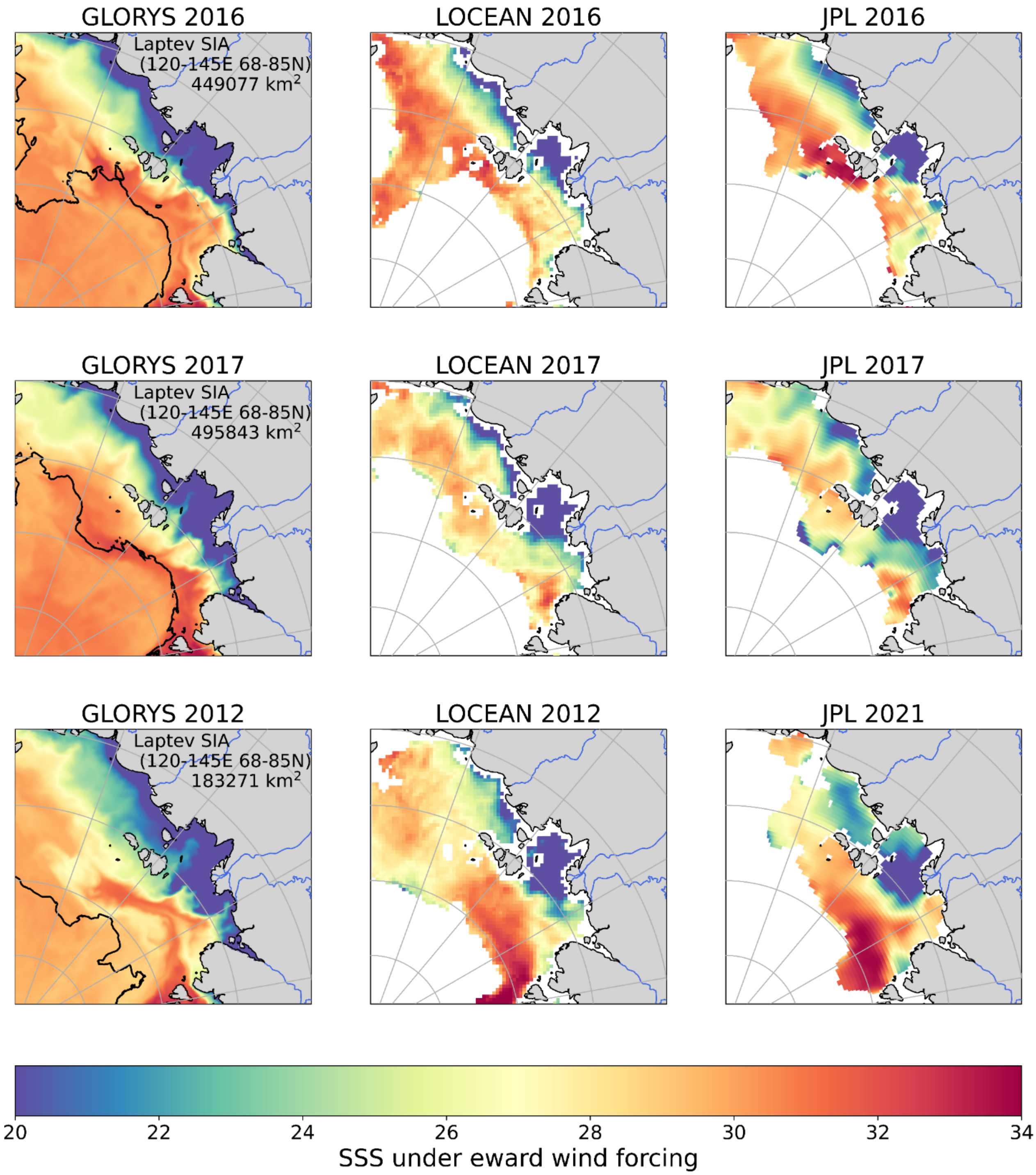

Figure A2: Years of eastward wind forcing for all years used to calculate eastward composites for (left to right) GLORYS12V1 SSS and LOCEAN SMOS (2016, 2017, 2012) and for JPL SMAP (2016, 2017, 2021). The GLORYS12V1 mean 30% sea ice concentration contour and mean GLORYS12V1 sea ice area (SIA) in the Laptev Sea (120-140, 68-85N) for each year shown is overlaid on that year's plot.

https://doi.org/10.5194/egusphere-2023-1403
Preprint. Discussion started: 28 June 2023
© Author(s) 2023. CC BY 4.0 License.

Data availability

All data used in this study is open access. JPL and RSS SMAP SSS data can be obtained from the Podaac data portal. LOCEAN SMOS data is available on the CATDS portal and SMOS BEC product is available on the BEC (Barcelona Expert Center) web page. CCI satellite SST data are available from Sea Surface Temperature Data (surftemp.net). All reanalysis products are available through the CMEMS portal.

In-situ data from the UDASH database and from Bjork (2017) are accessible on the Pangea portal. In-situ data from the NABOS cruises are available from the Arctic Data Center. In-situ data from cruises in 2016 and 2019 can be found in the supplementary materials of (Osadchiev et al., 2021).

Author contribution

Phoebe Hudson: Conceptualisation, Methodology, Validation, Formal Analysis, Visualisation, Writing –original draft, review & editing.

Adrien Martin: Supervision, Funding acquisition, Conceptualisation, Analysis, Writing – review & editing.

Simon Josey: Supervision, Analysis, Writing – review & editing.

Alice Marzocchi: Supervision, Analysis, Writing – review & editing.

Athanasios Angeloudis: Supervision, Analysis, Writing – review & editing.

Competing interests

The authors declare no conflict of interest, either financial or personal, that may have influenced the work reported here.

Acknowledgements

PAH was supported by the Natural Environment Research Council (NERC) SENSE Centre for Doctoral Training (NE/T00939X/1).

https://doi.org/10.5194/egusphere-2023-1403
Preprint. Discussion started: 28 June 2023
© Author(s) 2023. CC BY 4.0 License.

References

Anderson, L. G., Jutterström, S., Kaltin, S., Jones, E. P., and Björk, G.: Variability in river runoff distribution in the Eurasian Basin of the Arctic Ocean, J. Geophys. Res. Oceans, 109, https://doi.org/10.1029/2003JC001773, 2004.

Are, F. and Reimnitz, E.: An Overview of the Lena River Delta Setting: Geology, Tectonics, Geomorphology, and Hydrology on JSTOR, 2000.

Armitage, T. W. K., Bacon, S., and Kwok, R.: Arctic Sea Level and Surface Circulation Response to the Arctic Oscillation, Geophys. Res. Lett., 45, 6576–6584, https://doi.org/10.1029/2018GL078386, 2018.

Bauch, D., Gröger, M., Dmitrenko, I., Hölemann, J., Kirillov, S., Mackensen, A., Taldenkova, E., and Andersen, N.: Atmospheric controlled freshwater release at the Laptev Sea continental margin, Polar Res., https://doi.org/10.3402/polar.v30i0.5858, 2010.

Bauch, D., Hölemann, J. A., Nikulina, A., Wegner, C., Janout, M. A., Timokhov, L. A., and Kassens, H.: Correlation of river water and local sea-ice melting on the Laptev Sea shelf (Siberian Arctic), J. Geophys. Res. Oceans, 118, 550–561, https://doi.org/10.1002/jgrc.20076, 2013.

Baumann, T. M., Polyakov, I. V., Pnyushkov, A. V., Rember, R., Ivanov, V. V., Alkire, M. B., Goszczko, I., and Carmack, E. C.: On the Seasonal Cycles Observed at the Continental Slope of the Eastern Eurasian Basin of the Arctic Ocean, J. Phys. Oceanogr., 48, 1451–1470, https://doi.org/10.1175/JPO-D-17-0163.1, 2018.

Biló, T. C., Straneo, F., Holte, J., and Le Bras, I. a.-A.: Arrival of New Great Salinity Anomaly Weakens Convection in the Irminger Sea, Geophys. Res. Lett., 49, e2022GL098857, https://doi.org/10.1029/2022GL098857, 2022.

Charette, M. A., Kipp, L. E., Jensen, L. T., Dabrowski, J. S., Whitmore, L. M., Fitzsimmons, J. N., Williford, T., Ulfsbo, A., Jones, E., Bundy, R. M., Vivancos, S. M., Pahnke, K., John, S. G., Xiang, Y., Hatta, M., Petrova, M. V., Heimbürger-Boavida, L.-E., Bauch, D., Newton, R., Pasqualini, A., Agather, A. M., Amon, R. M. W., Anderson, R. F., Andersson, P. S., Benner, R., Bowman, K. L., Edwards, R. L., Gdaniec, S., Gerringa, L. J. A., González, A. G., Granskog, M., Haley, B., Hammerschmidt, C. R., Hansell, D. A., Henderson, P. B., Kadko, D. C., Kaiser, K., Laan, P., Lam, P. J., Lamborg, C. H., Levier, M., Li, X., Margolin, A. R., Measures, C., Middag, R., Millero, F. J., Moore, W. S., Paffrath, R., Planquette, H., Rabe, B., Reader, H., Rember, R., Rijkenberg, M. J. A., Roy-Barman, M., Rutgers van der Loeff, M., Saito, M., Schauer, U., Schlosser, P., Sherrell, R. M., Shiller, A. M., Slagter, H., Sonke, J. E., Stedmon, C., Woosley, R. J., Valk, O., van Ooijen, J., and Zhang, R.: The Transpolar Drift as a Source of Riverine and Shelf-Derived Trace Elements to the Central Arctic Ocean, J. Geophys. Res. Oceans, 125, e2019JC015920, https://doi.org/10.1029/2019JC015920, 2020.

Dean, K. G., Stringer, W. J., Ahlnas, K., Searcy, C., and Weingartner, T.: The influence of river discharge on the thawing of sea ice, Mackenzie River Delta: albedo and temperature analyses, Polar Res., 13, 83–94, https://doi.org/10.1111/j.1751-8369.1994.tb00439.x, 1994.

Dmitrenko, I., Kirillov, S., Eicken, H., and Markova, N.: Wind-driven summer surface hydrography of the eastern Siberian shelf, Geophys. Res. Lett., 32, https://doi.org/10.1029/2005GL023022, 2005.

Dmitrenko, I. A., Kirillov, S. A., and Tremblay, L. B.: The long-term and interannual variability of summer fresh water storage over the eastern Siberian shelf: Implication for climatic change, J. Geophys. Res. Oceans, 113, https://doi.org/10.1029/2007JC004304, 2008.

https://doi.org/10.5194/egusphere-2023-1403
Preprint. Discussion started: 28 June 2023
© Author(s) 2023. CC BY 4.0 License.

Dong, J., Shi, X., Gong, X., Astakhov, A. S., Hu, L., Liu, X., Yang, G., Wang, Y., Vasilenko, Y., Qiao, S., Bosin, A., and Lohmann, G.: Enhanced Arctic sea ice melting controlled by larger heat discharge of mid-Holocene rivers, Nat. Commun., 13, 5368, https://doi.org/10.1038/s41467-022-33106-1, 2022.

Dossa, A. N., Alory, G., da Silva, A. C., Dahunsi, A. M., and Bertrand, A.: Global Analysis of Coastal Gradients of Sea Surface Salinity, Remote Sens., 13, 2507, https://doi.org/10.3390/rs13132507, 2021.

Dubinina, E. O., Kossova, S. A., Miroshnikov, A. Yu., and Kokryatskaya, N. M.: Isotope (δD, δ18O) systematics in waters of the Russian Arctic seas, Geochem. Int., 55, 1022–1032, https://doi.org/10.1134/S0016702917110052, 2017.

Fofonova, V., Androsov, A., Danilov, S., Janout, M., Sofina, E., and Wiltshire, K.: Semidiurnal tides in the Laptev Sea Shelf zone in the summer season, Cont. Shelf Res., 73, 119–132, https://doi.org/10.1016/j.csr.2013.11.010, 2014.

Font, J., Camps, A., Borges, A., Martín-Neira, M., Boutin, J., Reul, N., Kerr, Y. H., Hahne, A., and Mecklenburg, S.: SMOS: The Challenging Sea Surface Salinity Measurement From Space, Proc. IEEE, 98, 649–665, https://doi.org/10.1109/JPROC.2009.2033096, 2010.

Fournier, S., Vandemark, D., Gaultier, L., Lee, T., Jonsson, B., and Gierach, M. M.: Interannual Variation in Offshore Advection of Amazon-Orinoco Plume Waters: Observations, Forcing Mechanisms, and Impacts, J. Geophys. Res. Oceans, 122, 8966–8982, https://doi.org/10.1002/2017JC013103, 2017.

Fournier, S., Lee, T., Tang, W., Steele, M., and Olmedo, E.: Evaluation and Intercomparison of SMOS, Aquarius, and SMAP Sea Surface Salinity Products in the Arctic Ocean, Remote Sens., 11, 3043, https://doi.org/10.3390/rs11243043, 2019.

Gommenginger, C., Chapron, B., Hogg, A., Buckingham, C., Fox-Kemper, B., Eriksson, L., Soulat, F., Ubelmann, C., Ocampo-Torres, F., Nardelli, B. B., Griffin, D., Lopez-Dekker, F., Knudsen, P., Andersen, O. B., Stenseng, L., Stapleton, N., Perrie, W., Violante-Carvalho, N., Schulz-Stellenfleth, J., Woolf, D., Isern-Fontanet, J., Ardhuin, F., Klein, P. M., Mouche, A., Pascual, A., Capet, X., Hauser, D., Stoffelen, A., Morrow, R. A., Aouf, L., Breivik, Ø., Fu, L. L., Johannessen, J. A., Aksenov, Y., Bricheno, L., Hirschi, J., Martin, A. C., Martin, A. P., Nurser, G., Polton, J., Wolf, J., Johnsen, H., Soloviev, A., Jacobs, G., Collard, F., Groom, S. B., Kudryavstev, V., Wilkin, J. L., Navarro, V., Babanin, A., Martin, M. J., Siddorn, J., Saulter, A., Rippeth, T., Emery, W., Maximenko, N., Romeiser, R., Graber, H., Alvera-Azcárate, A., Hughes, C., Vandemark, D., da Silva, J., Van Leeuwen, P. J., Naveira-Gabarato, A., Gemmrich, J., Mahadevan, A., Marquez, J., Munro, Y., Doody, S., and Burbidge, G.: SEASTAR: A mission to study ocean submesoscale dynamics and small-scale atmosphere-ocean processes in coastal, shelf and polar seas, Front. Mar. Sci., 6, https://doi.org/10.3389/fmars.2019.00457, 2019.

Hall, S. B., Subrahmanyam, B., Nyadjro, E. S., and Samuelsen, A.: Surface freshwater fluxes in the arctic and subarctic seas during contrasting years of high and low summer sea ice extent, Remote Sens., 13, https://doi.org/10.3390/rs13081570, 2021.

Hersbach, H., Bell, B., Berrisford, P., Hirahara, S., Horányi, A., Muñoz-Sabater, J., Nicolas, J., Peubey, C., Radu, R., Schepers, D., Simmons, A., Soci, C., Abdalla, S., Abellan, X., Balsamo, G., Bechtold, P., Biavati, G., Bidlot, J., Bonavita, M., De Chiara, G., Dahlgren, P., Dee, D., Diamantakis, M., Dragani, R., Flemming, J., Forbes, R., Fuentes, M., Geer, A., Haimberger, L., Healy, S., Hogan, R. J., Hólm, E., Janisková, M., Keeley, S., Laloyaux, P., Lopez, P., Lupu, C., Radnoti, G., de Rosnay, P., Rozum, I., Vamborg, F., Villaume, S., and Thépaut, J.-N.: The ERA5 global reanalysis, Q. J. R. Meteorol. Soc., 146, 1999–2049, https://doi.org/10.1002/qj.3803, 2020.

Hölemann, J. A., Kirillov, S., Klagge, T., Novikhin, A., Kassens, H., and Timokhov, L.: Near-bottom water warming in the Laptev Sea in response to atmospheric and sea-ice conditions in 2007, Polar Res., 30, 6425, https://doi.org/10.3402/polar.v30i0.6425, 2011.

https://doi.org/10.5194/egusphere-2023-1403
Preprint. Discussion started: 28 June 2023
© Author(s) 2023. CC BY 4.0 License.

Hordoir, R., Skagseth, Ø., Ingvaldsen, R. B., Sandø, A. B., Löptien, U., Dietze, H., Gierisch, A. M. U., Assmann, K. M., Lundesgaard, Ø., and Lind, S.: Changes in Arctic Stratification and Mixed Layer Depth Cycle: A Modeling Analysis, J. Geophys. Res. Oceans, 127, e2021JC017270, https://doi.org/10.1029/2021JC017270, 2022.

Horner-Devine, A. R., Hetland, R. D., and MacDonald, D. G.: Mixing and Transport in Coastal River Plumes, Annu. Rev. Fluid Mech., 47, 569–594, https://doi.org/10.1146/annurev-fluid-010313-141408, 2015.

IPCC (Intergovernmental Panel on Climate Change): Special Report: The Ocean and Cryosphere in a Changing Climate (final draft), IPCC Summ. Policymalers, TBD, TBD, https://www.ipcc.ch/report/srocc/, 2019.

Janout, M., Hölemann, J., Juhls, B., Krumpen, T., Rabe, B., Bauch, D., Wegner, C., Kassens, H., and Timokhov, L.: Episodic warming of near-bottom waters under the Arctic sea ice on the central Laptev Sea shelf, Geophys. Res. Lett., 43, 264–272, https://doi.org/10.1002/2015GL066565, 2016.

Janout, M. A. and Lenn, Y.-D.: Semidiurnal Tides on the Laptev Sea Shelf with Implications for Shear and Vertical Mixing, J. Phys. Oceanogr., 44, 202–219, https://doi.org/10.1175/JPO-D-12-0240.1, 2014.

Janout, M. A., Aksenov, Y., Hölemann, J. A., Rabe, B., Schauer, U., Polyakov, I. V., Bacon, S., Coward, A. C., Karcher, M., Lenn, Y.-D., Kassens, H., and Timokhov, L.: Kara Sea freshwater transport through Vilkitsky Strait: Variability, forcing, and further pathways toward the western Arctic Ocean from a model and observations: KARA SEA FRESHWATER TRANSPORT, J. Geophys. Res. Oceans, 120, 4925–4944, https://doi.org/10.1002/2014JC010635, 2015.

Janout, M. A., Hölemann, J., Laukert, G., Smirnov, A., Krumpen, T., Bauch, D., and Timokhov, L.: On the Variability of Stratification in the Freshwater-Influenced Laptev Sea Region, Front. Mar. Sci., 7, https://doi.org/10.3389/fmars.2020.543489, 2020.

Jean-Michel, L., Eric, G., Romain, B.-B., Gilles, G., Angélique, M., Marie, D., Clément, B., Mathieu, H., Olivier, L. G., Charly, R., Tony, C., Charles-Emmanuel, T., Florent, G., Giovanni, R., Mounir, B., Yann, D., and Pierre-Yves, L. T.: The Copernicus Global 1/12° Oceanic and Sea Ice GLORYS12 Reanalysis, Front. Earth Sci., 9, 2021.

Johnson, M. A. and Polyakov, I. V.: The Laptev Sea as a source for recent Arctic Ocean salinity changes, Geophys. Res. Lett., 28, 2017–2020, https://doi.org/10.1029/2000GL012740, 2001.

Juhls, B., Stedmon, C. A., Morgenstern, A., Meyer, H., Hölemann, J., Heim, B., Povazhnyi, V., and Overduin, P. P.: Identifying Drivers of Seasonality in Lena River Biogeochemistry and Dissolved Organic Matter Fluxes, Front. Environ. Sci., 8, 2020.

Kerr, Y. H., Waldteufel, P., Wigneron, J. P., Delwart, S., Cabot, F., Boutin, J., Escorihuela, M. J., Font, J., Reul, N., Gruhier, C., Juglea, S. E., Drinkwater, M. R., Hahne, A., Martin-Neira, M., and Mecklenburg, S.: The SMOS L: New tool for monitoring key elements ofthe global water cycle, Proc. IEEE, 98, 666–687, https://doi.org/10.1109/JPROC.2010.2043032, 2010.

Kraineva, M. V. and Golubeva, E. N.: Formation of Temperature Anomalies in the Laptev Sea (2000–2020 Years), in: Processes in GeoMedia—Volume V, edited by: Chaplina, T., Springer International Publishing, Cham, 169–178, https://doi.org/10.1007/978-3-030-85851-3_19, 2022.

Kubryakov, A., Stanichny, S., and Zatsepin, A.: River plume dynamics in the Kara Sea from altimetry-based lagrangian model, satellite salinity and chlorophyll data, Remote Sens. Environ., 176, 177–187, https://doi.org/10.1016/j.rse.2016.01.020, 2016.

Lagerloef, G., Colomb, F. R., Le Vine, D., Wentz, F., Yueh, S., Ruf, C., Lilly, J., Gunn, J., Chao, Y., deCharon, A., Feldman, G., and Swift, C.: The Aquarius/SAC-D Mission: Designed to Meet the Salinity Remote-Sensing Challenge, Oceanography, 21, 68–81, https://doi.org/10.5670/oceanog.2008.68, 2008.

https://doi.org/10.5194/egusphere-2023-1403
Preprint. Discussion started: 28 June 2023
© Author(s) 2023. CC BY 4.0 License.

Lee, T., Gille, S., Ardhuin, F., Boland, J., Bourassa, M., Chang, P., Cravatte, S., Farrar, T., Fewings, M., Jacobs, G., Jelenak, Z., Lyard, F., May, J., Remy, E., Renault, L., Rodriguez, E., Ubelmann, C., Bôas, B. V., and Wineteer, A.: A satellite mission concept to unravel small-scale ocean dynamics and air-sea interactions: ODYSEA (Ocean Dynamics and Surface Exchange with the Atmosphere), Copernicus Meetings, https://doi.org/10.5194/egusphere-egu23-4875, 2023.

Lentz, S. J. and Helfrich, K. R.: Buoyant gravity currents along a sloping bottom in a rotating fluid, J. Fluid Mech., 464, 251–278, https://doi.org/10.1017/S0022112002008868, 2002.

Liu, Y., Wang, J., Han, G., Lin, X., Yang, G., and Ji, Q.: Spatio-temporal analysis of east greenland polar front, Front. Mar. Sci., 9, 2022.

Martínez, J., Gabarró, C., Turiel, A., González-Gambau, V., Umbert, M., Hoareau, N., González-Haro, C., Olmedo, E., Arias, M., Catany, R., Bertino, L., Raj, R. P., Xie, J., Sabia, R., and Fernández, D.: Improved BEC SMOS Arctic Sea Surface Salinity product v3.1, Earth Syst. Sci. Data Discuss., 1–28, https://doi.org/10.5194/essd-2021-334, 2021.

Masina, S., Storto, A., Ferry, N., Valdivieso, M., Haines, K., Balmaseda, M., Zuo, H., Drevillon, M., and Parent, L.: An ensemble of eddy-permitting global ocean reanalyses from the MyOcean project, Clim. Dyn., 49, 813–841, https://doi.org/10.1007/s00382-015-2728-5, 2017.

Merchant, C. J., Embury, O., Bulgin, C. E., Block, T., Corlett, G. K., Fiedler, E., Good, S. A., Mittaz, J., Rayner, N. A., Berry, D., Eastwood, S., Taylor, M., Tsushima, Y., Waterfall, A., Wilson, R., and Donlon, C.: Satellite-based time-series of sea-surface temperature since 1981 for climate applications, Sci. Data, 6, https://doi.org/10.1038/s41597-019-0236-x, 2019.

Morison, J., Kwok, R., Peralta-Ferriz, C., Alkire, M., Rigor, I., Andersen, R., and Steele, M.: Changing Arctic Ocean freshwater pathways, Nature, 481, 66–70, https://doi.org/10.1038/nature10705, 2012.

Morison, J., Kwok, R., Dickinson, S., Andersen, R., Peralta Ferriz, C., Morison, D., Rigor, I., Dewey, S., and Guthrie, J.: The Cyclonic Mode of Arctic Ocean Circulation, J. Phys. Oceanogr., https://doi.org/10.1175/JPO-D-20-0190.1, 2021.

Morrow, R., Fu, L.-L., Ardhuin, F., Benkiran, M., Chapron, B., Cosme, E., d'Ovidio, F., Farrar, J. T., Gille, S. T., Lapeyre, G., Le Traon, P.-Y., Pascual, A., Ponte, A., Qiu, B., Rascle, N., Ubelmann, C., Wang, J., and Zaron, E. D.: Global Observations of Fine-Scale Ocean Surface Topography With the Surface Water and Ocean Topography (SWOT) Mission, Front. Mar. Sci., 6, 2019.

Nicolì, D., Bellucci, A., Iovino, D., Ruggieri, P., and Gualdi, S.: The impact of the AMV on Eurasian summer hydrological cycle, Sci. Rep., 10, 14444, https://doi.org/10.1038/s41598-020-71464-2, 2020.

Nielsen, D. M., Dobrynin, M., Baehr, J., Razumov, S., and Grigoriev, M.: Coastal Erosion Variability at the Southern Laptev Sea Linked to Winter Sea Ice and the Arctic Oscillation, Geophys. Res. Lett., 47, e2019GL086876, https://doi.org/10.1029/2019GL086876, 2020.

Nummelin, A., Ilicak, M., Li, C., and Smedsrud, L. H.: Consequences of future increased Arctic runoff on Arctic Ocean stratification, circulation, and sea ice cover, J. Geophys. Res. Oceans, 121, 617–637, https://doi.org/10.1002/2015JC011156, 2016.

Ogi, M., Rysgaard, S., and Barber, D. G.: Importance of combined winter and summer Arctic Oscillation (AO) on September sea ice extent, Environ. Res. Lett., 11, 034019, https://doi.org/10.1088/1748-9326/11/3/034019, 2016.

https://doi.org/10.5194/egusphere-2023-1403
Preprint. Discussion started: 28 June 2023
© Author(s) 2023. CC BY 4.0 License.

Olmedo, E., Gabarró, C., González-Gambau, V., Martínez, J., Ballabrera-Poy, J., Turiel, A., Portabella, M., Fournier, S., and Lee, T.: Seven Years of SMOS Sea Surface Salinity at High Latitudes: Variability in Arctic and Sub-Arctic Regions, Remote Sens., 10, 1772, https://doi.org/10.3390/rs10111772, 2018.

Osadchiev, A., Frey, D., Spivak, E., Shchuka, S., Tilinina, N., and Semiletov, I.: Structure and Inter-Annual Variability of the Freshened Surface Layer in the Laptev and East-Siberian Seas During Ice-Free Periods, Front. Mar. Sci., 8, 1871, https://doi.org/10.3389/fmars.2021.735011, 2021.

Overland, J. E. and Wang, M.: Large-scale atmospheric circulation changes are associated with the recent loss of Arctic sea ice, Tellus A, 62, 1–9, https://doi.org/10.1111/j.1600-0870.2009.00421.x, 2010.

Paffrath, R., Laukert, G., Bauch, D., Rutgers van der Loeff, M., and Pahnke, K.: Separating individual contributions of major Siberian rivers in the Transpolar Drift of the Arctic Ocean, Sci. Rep., 11, 8216, https://doi.org/10.1038/s41598-021-86948-y, 2021.

Park, H., Watanabe, E., Kim, Y., Polyakov, I., Oshima, K., Zhang, X., Kimball, J. S., and Yang, D.: Increasing riverine heat influx triggers Arctic sea ice decline and oceanic and atmospheric warming, Sci. Adv., 6, eabc4699, https://doi.org/10.1126/sciadv.abc4699, 2020.

Pasternak, A., Drits, A., Arashkevich, E., and Flint, M.: Differential Impact of the Khatanga and Lena (Laptev Sea) Runoff on the Distribution and Grazing of Zooplankton, Front. Mar. Sci., 9, 2022.

Piepmeier, J. R., Focardi, P., Horgan, K. A., Knuble, J., Ehsan, N., Lucey, J., Brambora, C., Brown, P. R., Hoffman, P. J., French, R. T., Mikhaylov, R. L., Kwack, E.-Y., Slimko, E. M., Dawson, D. E., Hudson, D., Peng, J., Mohammed, P. N., De Amici, G., Freedman, A. P., Medeiros, J., Sacks, F., Estep, R., Spencer, M. W., Chen, C. W., Wheeler, K. B., Edelstein, W. N., O'Neill, P. E., and Njoku, E. G.: SMAP L-Band Microwave Radiometer: Instrument Design and First Year on Orbit, IEEE Trans. Geosci. Remote Sens., 55, 1954–1966, https://doi.org/10.1109/tgrs.2016.2631978, 2017.

Polyakov, I. and Rember, R.: Conductivity, Temperature, Pressure (CTD) measurements from cast data taken in the Eurasian and Makarov basins, Arctic Ocean, 2018, https://doi.org/10.18739/A2X34MS0V, 2019.

Polyakov, I. V., Beszczynska, A., Carmack, E. C., Dmitrenko, I. A., Fahrbach, E., Frolov, I. E., Gerdes, R., Hansen, E., Holfort, J., Ivanov, V. V., Johnson, M. A., Karcher, M., Kauker, F., Morison, J., Orvik, K. A., Schauer, U., Simmons, H. L., Skagseth, Ø., Sokolov, V. T., Steele, M., Timokhov, L. A., Walsh, D., and Walsh, J. E.: One more step toward a warmer Arctic, Geophys. Res. Lett., 32, 1–4, https://doi.org/10.1029/2005GL023740, 2005.

Polyakova, Y., Kryukova, I., Martynov, F., Novikhin, A., Abramova, E., Kassens, H., and Hoelemann, J.: Community structure and spatial distribution of phytoplankton in relation to hydrography in the Laptev Sea and the East Siberian Sea (autumn 2008), Polar Biol., 44, https://doi.org/10.1007/s00300-021-02873-w, 2021.

Preußer, A., Ohshima, K. I., Iwamoto, K., Willmes, S., and Heinemann, G.: Retrieval of Wintertime Sea Ice Production in Arctic Polynyas Using Thermal Infrared and Passive Microwave Remote Sensing Data, J. Geophys. Res. Oceans, 124, 5503–5528, https://doi.org/10.1029/2019JC014976, 2019.

Prowse, T., Bring, A., M\aard, J., and Carmack, E.: Arctic freshwater synthesis: Introduction, J. Geophys. Res. G Biogeosciences, 120, 2121–2131, https://doi.org/10.1002/2015JG003127, 2015.

Rabe, B., Karcher, M., Kauker, F., Schauer, U., Toole, J. M., Krishfield, R. A., Pisarev, S., Kikuchi, T., and Su, J.: Arctic Ocean basin liquid freshwater storage trend 1992–2012, Geophys. Res. Lett., 41, 961–968, https://doi.org/10.1002/2013GL058121, 2014.

© Author(s) 2023. CC BY 4.0 License.

Reimnitz, E., Dethleff, D., and Nürnberg, D.: Contrasts in Arctic shelf sea-ice regimes and some implications: Beaufort Sea versus Laptev Sea, Mar. Geol., 119, 215–225, https://doi.org/10.1016/0025-3227(94)90182-1, 1994.

Reul, N., Grodsky, S. A., Arias, M., Boutin, J., Catany, R., Chapron, B., D'Amico, F., Dinnat, E., Donlon, C., Fore, A., Fournier, S., Guimbard, S., Hasson, A., Kolodziejczyk, N., Lagerloef, G., Lee, T., Le Vine, D. M., Lindstrom, E., Maes, C., Mecklenburg, S., Meissner, T., Olmedo, E., Sabia, R., Tenerelli, J., Thouvenin-Masson, C., Turiel, A., Vergely, J. L., Vinogradova, N., Wentz, F., and Yueh, S.: Sea surface salinity estimates from spaceborne L-band radiometers: An overview of the first decade of observation (2010–2019), Remote Sens. Environ., 242, 111769, https://doi.org/10.1016/j.rse.2020.111769, 2020.

Shakhova, N., Semiletov, I., Leifer, I., Sergienko, V., Salyuk, A., Kosmach, D., Chernykh, D., Stubbs, C., Nicolsky, D., Tumskoy, V., and Gustafsson, Ö.: Ebullition and storm-induced methane release from the East Siberian Arctic Shelf, Nat. Geosci., 7, 64–70, https://doi.org/10.1038/ngeo2007, 2014.

Shiklomanov, A., Déry, S., Tretiakov, M., Yang, D., Magritsky, D., Georgiadi, A., and Tang, W.: River Freshwater Flux to the Arctic Ocean, in: Arctic Hydrology, Permafrost and Ecosystems, edited by: Yang, D. and Kane, D. L., Springer International Publishing, Cham, 703–738, https://doi.org/10.1007/978-3-030-50930-9_24, 2021.

Stadnyk, T. A., Tefs, A., Broesky, M., Déry, S. J., Myers, P. G., Ridenour, N. A., Koenig, K., Vonderbank, L., and Gustafsson, D.: Changing freshwater contributions to the Arctic: A 90-year trend analysis (1981–2070), Elem. Sci. Anthr., 9, https://doi.org/10.1525/elementa.2020.00098, 2021.

Steele, M. and Ermold, W.: Salinity trends on the Siberian shelves, Geophys. Res. Lett., 31, https://doi.org/10.1029/2004GL021302, 2004.

Suess, M., De Witte, E., and Rommen, B.: Earth Explorer 10 Candidate Mission Harmony, in: EUSAR 2022; 14th European Conference on Synthetic Aperture Radar, EUSAR 2022; 14th European Conference on Synthetic Aperture Radar, 1–4, 2022.

Supply, A., Boutin, J., Vergely, J.-L., Kolodziejczyk, N., Reverdin, G., Reul, N., and Tarasenko, A.: New insights into SMOS sea surface salinity retrievals in the Arctic Ocean, Remote Sens. Environ., 249, 112027, https://doi.org/10.1016/j.rse.2020.112027, 2020.

Tang, W., Yueh, S., Yang, D., Fore, A., Hayashi, A., Lee, T., Fournier, S., and Holt, B.: The Potential and Challenges of Using Soil Moisture Active Passive (SMAP) Sea Surface Salinity to Monitor Arctic Ocean Freshwater Changes, Remote Sens., 10, 869, https://doi.org/10.3390/rs10060869, 2018.

Tarasenko, A., Supply, A., Kusse-Tiuz, N., Ivanov, V., Makhotin, M., Tournadre, J., Chapron, B., Boutin, J., Kolodziejczyk, N., and Reverdin, G.: Properties of surface water masses in the Laptev and the East Siberian seas in summer 2018 from in situ and satellite data, Ocean Sci., 17, 221–247, https://doi.org/10.5194/os-17-221-2021, 2021.

Thibodeau, B., Bauch, D., Kassens, H., and Timokhov, L. A.: Interannual variations in river water content and distribution over the Laptev Sea between 2007 and 2011: The Arctic Dipole connection, Geophys. Res. Lett., 41, 7237–7244, https://doi.org/10.1002/2014GL061814, 2014.

Timokhov, L. A.: Regional characteristics of the Laptev and the East Siberian seas: climate, topography, ice phases, thermohaline regime, circulation, Berichte Zur Polarforsch., 144, 15–31, 1994.

Umbert, M., Gabarro, C., Olmedo, E., Gonçalves-Araujo, R., Guimbard, S., and Martinez, J.: Using Remotely Sensed Sea Surface Salinity and Colored Detrital Matter to Characterize Freshened Surface Layers in the Kara and Laptev Seas during the Ice-Free Season, Remote Sens., https://doi.org/10.3390/rs13193828, 2021.

© Author(s) 2023. CC BY 4.0 License.

Vinogradova, N., Lee, T., Boutin, J., Drushka, K., Fournier, S., Sabia, R., Stammer, D., Bayler, E., Reul, N., Gordon, A., Melnichenko, O., Li, L., Hackert, E., Martin, M., Kolodziejczyk, N., Hasson, A., Brown, S., Misra, S., and Lindstrom, E.: Satellite Salinity Observing System: Recent Discoveries and the Way Forward, Front. Mar. Sci., 6, https://doi.org/10.3389/fmars.2019.00243, 2019.

Wang, P., Huang, Q., Pozdnyakov, S., Liu, S., Ma, N., Wang, T., Zhang, Y., Yu, J., Xie, J., Fu, G., Frolova, N., and Liu, C.: Potential role of permafrost thaw on increasing Siberian river discharge, Environ. Res. Lett., 16, 034046, https://doi.org/10.1088/1748-9326/abe326, 2021.

Zatsepin, A. G., Kremenetskiy, V. V., Kubryakov, A. A., Stanichny, S. V., and Soloviev, D. M.: Propagation and transformation of waters of the surface desalinated layer in the Kara Sea, Oceanology, 55, 450–460, https://doi.org/10.1134/S0001437015040153, 2015.

Zhuk, V. R. and Kubryakov, A. A.: Interannual Variability of the Lena River Plume Propagation in 1993–2020 during the Ice-Free Period on the Base of Satellite Salinity, Temperature, and Altimetry Measurements, Remote Sens., 13, 4252, https://doi.org/10.3390/rs13214252, 2021.

Zika, J. D., Skliris, N., George Nurser, A. J., Josey, S. A., Mudryk, L., Laliberté, F., and Marsh, R.: Maintenance and broadening of the ocean's salinity distribution by the water cycle, J. Clim., 28, 9550–9560, https://doi.org/10.1175/JCLI-D-15-0273.1, 2015.